



Evaporation of sulphate aerosols at low relative humidity

Georgios Tsagkogeorgas¹, Pontus Roldin^{2,3}, Jonathan Duplissy^{2,4}, Linda Rondo⁵, Jasmin Tröstl⁶, Jay G. Slowik⁶, Sebastian Ehrhart^{5,a}, Alessandro Franchin², Andreas Kürten⁵, Antonio Amorim⁷, Federico Bianchi², Jasper Kirkby^{5,8}, Tuukka Petäjä², Urs Baltensperger⁶, Michael Boy², Joachim Curtius⁵, Richard C. Flagan⁹, Markku Kulmala^{2,4}, Neil M. Donahue¹⁰, Frank Stratmann¹

¹Leibniz Institute for Tropospheric Research, 04318, Leipzig, Germany

²Department of Physics, University of Helsinki, P.O. Box 64, 00014, Helsinki, Finland

³Division of Nuclear Physics, Lund University, P.O. Box 118, 221 00, Lund, Sweden

⁴Helsinki Institute of Physics, University of Helsinki, P.O. Box 64, 00014 Helsinki, Finland

10 ⁵Institute for Atmospheric and Environmental Sciences, Goethe University Frankfurt, 60438, Frankfurt am Main, Germany

⁶Paul Scherrer Institute, CH-5232, Villigen, Switzerland

⁷Fac. Ciências & CENTRA, Universidade de Lisboa, Campo Grande, 1749-016, Lisboa, Portugal

⁸CERN, CH-1211, Geneva, Switzerland

⁹California Institute of Technology, Pasadena, CA 91125, USA

15 ¹⁰Center for Atmospheric Particle Studies, Carnegie Mellon University, Pittsburgh, PA 15213, USA

^anow at: Atmospheric Chemistry Department, Max Planck Institute for Chemistry, 55128, Mainz, Germany

Correspondence to: Georgios Tsagkogeorgas (george.tsagkogeorgas@tropos.de)

Abstract. Here we explore the vapour pressure of sulphuric acid at very low relative humidity, where evaporation of sulphuric acid from particles can be important in the atmospheres of Earth and Venus. We performed experiments in the CLOUD chamber at CERN forming sulphuric acid particles via nucleation and then measuring evaporation versus temperature and relative humidity. We modelled the experiments with the ADCHAM model to constrain the thermodynamic properties governing the evaporation of sulphuric acid. ADCHAM includes a thermodynamics module coupled to an aerosol dynamics module. We derived the mole fractions and activity coefficients of H₂SO₄, HSO₄⁻, SO₄²⁻ and SO₃ in the particles and then simulated the condensation and evaporation of H₂SO₄ and SO₃. We constrained the equilibrium constants for the dissociation of H₂SO₄ to HSO₄⁻ ($K_{H_2SO_4}$) and the dehydration of H₂SO₄ to SO₃ (${}^vK_{SO_3}$). Our results suggest that particle shrinkage is mainly governed by H₂SO₄ evaporation, however, we cannot dismiss a contribution from SO₃ evaporation. We conclude that $K_{H_2SO_4} = 2-4 \cdot 10^9 \text{ mol} \cdot \text{kg}^{-1}$ at $288.8 \pm 5 \text{ K}$ and ${}^vK_{SO_3} \geq 1.4 \cdot 10^{10}$.

Key words: sulphate aerosol evaporation, sulphuric acid dissociation, sulphuric acid equilibrium constants, sulphuric acid vapour pressure, water activity, activity coefficients, Earth's and Venus' stratospheres, CLOUD experiment

30 1 Introduction

Suspended particulate matter in the atmosphere plays a key role in Earth's climate. Atmospheric aerosol particles affect the amount of solar radiation absorbed by the Earth system. This is accomplished either when atmospheric aerosol particles directly absorb or scatter incoming solar energy (causing warming or cooling), or when particles act as cloud condensation or ice nuclei



(leading to an increase in cloud albedo, which causes cooling). A substantial fraction of particle number and mass across a wide range of environmental conditions arises from sulphur emissions (Clarke et al., 1998a; Turco et al., 1982). Sulphur in Earth's atmosphere in turn originates from natural phenomena like volcanic eruptions, biota decomposition, or human activities like coal combustion. Sulphur is also a crucial constituent in Venus' atmosphere, an environment with very low relative humidity (RH) (Moroz et al., 1979; Hoffman et al., 1980a), forming the main cloud layer in the form of sulphuric acid droplets (Donahue et al., 1982), which are maintained in an intricate photochemical cycle (photooxidation of carbonyl sulphide, Prinn 1973).

While sulphuric acid (H_2SO_4) is often presumed to be practically non-volatile, this is not always the case. There are several circumstances on Earth and Venus where the vapour pressure of H_2SO_4 matters; specifically, at very low RH, high temperature (T), when there is a deficit of stabilizing bases, and when particles are very small. A very important region of Earth's environment is the upper stratosphere where these conditions prevail (Vaida et al. 2003). Under these conditions H_2SO_4 can evaporate from particles. This can either inhibit growth of nanoparticles or lead them to shrink, depending on circumstances.

Furthermore, molecular H_2SO_4 is never the dominant constituent in sulphuric acid solutions. It will completely dehydrate to sulphur trioxide (SO_3 , which is extremely volatile) in a truly dry system and yet almost entirely dissociate into bisulphate ion (HSO_4^-) and hydronium cation (H_3O^+) in the presence of even trace water (H_2O) (Clegg and Brimblecombe, 1995). This is why H_2SO_4 is such a powerful desiccant. Also, bases such as ammonia (NH_3) and possibly extremely low volatility organic compounds (ELVOCs) will enhance chemical stabilization and form sulphate salts. The thermodynamics of the H_2SO_4 - H_2O system at low RH are uncertain, so we seek to improve our understanding of this part of the phase diagram. To accomplish this, we measured shrinkage of nearly pure H_2SO_4 particles in the CLOUD chamber at CERN at very low RH and then simulated these experiments with an aerosol dynamics model coupled with a thermodynamics model to constrain the equilibrium constants, for the dissociation $K_{\text{H}_2\text{SO}_4}$ and the dehydration $^xK_{\text{SO}_3}$, of H_2SO_4 coupling HSO_4^- , H_2SO_4 , and SO_3 . These new values can be used in models that simulate the evolution of sulphate aerosol particles in Venus' and Earth's stratospheres.

2 H_2SO_4 presence on atmospheres of terrestrial planets and chemistry

2.1 Venus: a terrestrial planet with a sulphur composed atmosphere

Venus' atmosphere maintains a cloud layer consisting of a H_2SO_4 - H_2O solution surrounding the planet. In the upper troposphere, 50 km to ~65 km above surface, the Venusian thick clouds consist of sulphur dioxide (SO_2) and H_2SO_4 (Krasnopolsky and Parshev, 1981; Krasnopolsky, 2006b). Above the altitude of 70 km extends an upper haze layer (Esposito et al., 1983) very similar to Earth's stratospheric sulphate layer. The effective formation of the cloud cover and haze layer are the result of the ability of H_2SO_4 to readily condense due to its low vapour pressure. Sulphuric acid's reaction paths remain a subject of investigation (Zhang et al., 2010), which makes the study of the sulphur cycle (including the sulphur species SO,



SO₂, SO₃, H₂SO₄) an important endeavour for understanding both the chemistry and climate of Venus (Mills et al., 2007; Hashimoto and Abe, 2000).

2.2 Natural and anthropogenic sulphate aerosol formation on Earth

In Earth's troposphere, the three main natural agents for sulphate aerosol formation are dimethyl sulphide (DMS), which arises from marine phytoplankton decomposition (Charlson et al., 1987; Kiene, 1999; Simó and Pedrós–Alió, 1999), SO₂, which occurs naturally as a decay product of plant and animal matter (Grädel and Crutzen, 1994; Hübert, 1999; Capaldo et al., 1999), and carbonyl sulphide (OCS), which is emitted from anaerobic biological activity and provides the main non–volcanic flux of sulphur into the stratosphere (Galloway and Rodhe, 1991; Rhode, 1999).

Another important natural source arises from the volcanic activity. Violent volcanic eruptions can loft SO₂ to the stratosphere, and the SO₂ can then form aerosol particles containing sulphur. As these stratospheric sulphur aerosol particles are above most clouds, they can remain suspended in the stratosphere for ~2y before falling into the troposphere (Wilson et al., 1993) or less (0.8–1.5y depending on a variety of parameters, Deshler, 2008).

The atmospheric sulphate burden is substantially perturbed by sulphur emissions associated with anthropogenic activities. By far the largest anthropogenic source of sulphur is fossil–fuel combustion; coal is the predominant source, but also heavy fuel oil is important (Öm et al., 1996; Smith et al., 2001). Fossil–fuel combustion constitutes ~²/₃ of the total global sulphur flux to the atmosphere (Rhode, 1999; Wen and Carignan, 2007), and dominates emissions in most populated regions. Other anthropogenic factors also affect the H₂SO₄ budget, notably sulphur aerosol formation in aircraft plumes, and extensive sulphur use in industry.

Aircraft emissions are a minor fraction of the global burden, but, because they occur high in the free troposphere or lower stratosphere, they can still have a disproportionate effect on the planetary energy balance (Fahey et al., 1995, Miake–Lye et al., 1998). Prior studies have revealed that fuel sulphur accounts for a large fraction of the atmospheric aerosol (Hofmann and Rosen, 1978), and have shown efficient fuel sulphur conversion into particulate H₂SO₄ (Fahey et al., 1995; Curtius et al., 1998), as well as substantial production of aqueous sulphate particles due to gas–to–particle conversion in aircraft plumes (Turco et al., 1982; Hofmann, 1991; Schumann et al., 1996). Moreover, simulations reveal that fuel combustion generates large numbers of volatile ultrafine sulphuric acid particles (Yu and Turco, 1998).

Sulphuric acid is also a major industrial chemical. Industrial manufacture of H₂SO₄ includes oxidation of SO₂ to SO₃ and subsequent dissolution of SO₃ in H₂SO₄ to form H₂SO_{4(aq)}; another technology employs decomposition of sulfuric acid containing wastes. The extensive use of the industrial product has a direct environmental impact in the microclimate. However, on a regional to global scale the acidification of fresh water and forest ecosystems is mainly caused by wet and dry deposition of SO₂ and sulphate particles (Simpson et al., 2006). Acid rain is produced when SO₂ is dissolved in cloud and rain droplets and is oxidized by H₂O₂ and O₃ in the aqueous phase to produce sulphur with the oxidation state +6, S(VI).



2.3 Global presence of sulphate particles and their effect on Earth's climate

Sulphate particles are present throughout the atmosphere, forming a permanent stratospheric aerosol or Junge layer (Junge et al., 1961), which is an important regulator of Earth's climate and of the abundance of stratospheric ozone (O₃). Most of the ultrafine stratospheric aerosol is sulphate (75–85 % wt H₂SO₄) (Junge, 1954, 1963), these particles form polar stratospheric clouds (Molina et al., 1993; Toon and Tolbert, 1995; Koop and Carslaw, 1996; Clarke et al., 1998b; Schreiner et al., 1999). Sulphate is also a major constituent of tropospheric aerosol, where H₂SO₄ is often neutralised by gaseous ammonia (NH_{3(g)}) (Marti et al., 1997; Finlayson-Pitts and Pitts, 1999; Jimenez et al., 2009,). The interfacial structure of sulphate aerosol provides heterogeneous reaction sites (Solomon, 1999), which, more than sites on ice, catalyse reactions implicated in O₃ depletion in various atmospheric regions. These include the mid-latitude stratosphere (Robinson et al., 1997; Bianco and Hynes, 1999; McNamara and Hillier, 2000), the Antarctic stratosphere (Hanson and Ravishankara, 1995), and the Arctic boundary layer (Fan and Jacobs, 1992; Abbatt and Nowack, 1997). The efficiency of sulphate aerosol relative to ice is due to the abundance of sulphuric acid and water vapour throughout the stratosphere, and its ability to react effectively at temperatures below ~195 K.

The net result of anthropogenic sulphur emissions since the industrial revolution is an uncertain cooling effect masking roughly one-third of the total warming effect associated with human greenhouse-gas emissions. This is split between direct scattering of light by aerosols and increased reflection of light from clouds whose properties have been altered by aerosols (IPCC, 2013). However, the residence time of aerosols ranges between roughly one week in the troposphere to less than two years in the stratosphere, while greenhouse gasses remain for decades to, for all practical purposes, forever. Consequently, while the high uncertainty of this aerosol masking limits our ability to quantify climate sensitivity to greenhouse-gas forcing, it would also abate rapidly when, and if the global anthropogenic sulphur emissions were curtailed, causing a suddenly increased climate forcing with potentially severe consequences. Recent Earth-system model simulations show that the sulfate aerosol reduction in Europe since 1980 may be one of the main reasons for the observed amplified Arctic warming since that time (Acosta Navarro *et al.*, 2016).

2.4 Importance of the low sulphuric acid vapour pressure in atmospheric studies

H₂SO₄ serves as an effective nucleating species and, thus, strongly influences atmospheric new-particle formation (Laaksonen and Kulmala, 1991; Weber et al., 1999; Kulmala et al., 2000; Yu and Turco, 2001; Fiedler et al., 2005; Kuang et al., 2008). New-particle formation via gas-to-particle conversion produces most of particles in the global atmosphere (Kulmala et al., 2004; Merikanto et al., 2009), and can constitute about half of the global cloud condensation nuclei (CCN) inventory (Yu and Luo, 2009, Pierce and Adams 2009). The nucleation rate, which is the formation rate (cm⁻³·s⁻¹) of new particles at the critical size, strongly depends upon the saturation ratio of H₂SO₄, which is the ratio of the actual H₂SO₄ vapour pressure to the saturation vapour pressure over a flat surface of pure H₂SO₄. Uncertainty in this ratio results in an uncertainty of several orders of magnitude in the calculated nucleation rate (Roedel, 1979). To model the excess H₂SO₄ responsible for the gas-to-particle



conversion prerequisite is the precision regarding the vapour pressure of H_2SO_4 over sulphuric acid and/or neutralized solutions.

The sulphuric acid vapour pressure appears through the free-energy term in the exponent of the new-particle formation rate (Volmer and Weber, 1926; Stauffer, 1976). Quantitative theoretical predictions of nucleation rates are highly uncertain because the pure H_2SO_4 equilibrium vapour pressure is not well known. Suggested values range from $1.3 \cdot 10^{-9}$ to $5 \cdot 10^{-7}$ atm at 298 K, (Gmitro and Vermeulen, 1964; Doyle, 1961; Kiang and Stauffer, 1973). Many studies have described sulphuric-acid vapour-pressure measurements over unneutralized, concentrated $\text{H}_2\text{SO}_{4(aq)}$ solutions (>90 % acid by weight) at temperatures higher than those encountered in the atmosphere (>323 K) (Roedel, 1979; Ayers et al., 1980; Richardson et al., 1986). The thermodynamic derivation of the H_2SO_4 vapour pressure using pure-component thermodynamic values of Giaque et al. (1960) without sufficient experimental constraints included unreliable extrapolations while attempting to establish vapour-pressure relations among the components of sulphuric-acid solutions. A later extrapolation of the experimental equilibrium vapour pressure expression of Ayers et al. (1980) to ambient temperatures (Kulmala and Laksonen, 1990) mainly applies in binary nucleation calculations (Vehkamäki et al., 2002). At 300–333 K, the H_2SO_4 vapour pressure over mixed $\text{H}_2\text{SO}_{4(aq)}\text{--}(\text{NH}_4)_2\text{SO}_4$ solutions drops significantly as the $[\text{NH}_4^+]:[\text{SO}_4^{2-}]$ exceeds 0.5 (Marti et al., 1997). However, accurate calculations of the H_2SO_4 vapour pressure require accurate equilibrium rate constant values to constrain the reactions of formation and dissociation of H_2SO_4 in aqueous solutions.

2.5 Aqueous phase sulphuric acid reactions

H_2SO_4 dissociation and potential dehydration to SO_3 are the principal subjects of this study. In aqueous solutions H_2SO_4 can dissociate in two steps.



H_2SO_4 partially dissociates to form HSO_4^- via reaction 1 (R1). $K_{\text{H}_2\text{SO}_4}$ represents the equilibrium constant for R1. HSO_4^- can then undergo a second dissociation reaction (R2) to form a sulphate ion (SO_4^{2-}). In above reactions, sulphur's oxidation number is 6 (S(VI)).

For dilute aqueous solutions, R1 is considered to be complete. However, when the mole fraction of S(VI) exceeds ~0.5, H_2SO_4 can be detected in the solution (Walrafen et al., 2000; Margarela et al., 2013). When H_2SO_4 is present in the solution, dehydration of H_2SO_4 to form SO_3 (R3) can also be important (Wang et al., 2006; Que et al., 2011). ${}^xK_{\text{SO}_3}$ represents the equilibrium constant for R3 on a mole fraction basis.



NH_3 , which mainly originates from anthropogenic agriculture emissions, is the most abundant base in atmospheric



secondary aerosol particles. NH_3 neutralises sulphuric acid particles by reacting with H^+ and forming an ammonium ion (NH_4^+) (R4).



Even in the cleanest environments NH_3 is present at low concentrations and $\text{NH}_{3(g)}$ will be taken up during the growth of acidic sulphate particles.

3 Methods

In the CLOUD (Cosmics Leaving Outdoor Droplets, Kirkby et al. (2011)) chamber at CERN, we measured the H_2SO_4 aerosol evaporation process under precisely controlled temperature and relative humidity. We designed experiments to accomplish a gradual decrease of RH (from 11.0 to 0.3 %) under atmospherically relevant conditions.

3.1 Experimental set up

3.1.1 The CLOUD chamber

Details of the CLOUD chamber, the main element of the experimental set up can be found in Kirkby et al. (2011) and Duplissy et al. (2016). Briefly, the CLOUD chamber is a 26.1 m³ electro-polished stainless-steel cylindrical continuously stirred tank reactor that enables aerosol experiments under the full range of tropospheric conditions. The chamber temperature is controlled by air circulating in the space between the chamber wall and its surrounding thermal housing, allowing measurement at a high standard accuracy of ± 0.1 K from 200 K to 373 K. The nominal operating pressure of the chamber is one atmosphere. Ultra-pure dry air is generated by the evaporation of cryogenic liquid nitrogen (N_2) and liquid oxygen (O_2) to produce a 79:21 mixture. A controlled portion of the ultra-pure dry air flow passes through a Nafion humidifier and is then mixed with ultra-pure dry air. By precisely adjusting the temperature and air flow through the Nafion humidifier, the RH in the CLOUD chamber is accurately controlled (Duplissy et al. 2016). Two other dedicated inlet systems are used for O_3 and SO_2 . Complete mixing of the gases in the chamber is ensured by two fans, one at the top of the chamber, and the other at the bottom, running in counterflow (Voigtlander et al., 2012). All gas pipes are stainless steel to avoid contamination; and gas seals are chemically inert gold coated metal. As a result, we achieve extremely clean conditions in the CLOUD chamber (Schnitzhofer et al., 2014; Bianchi et al., 2012), unless we have intentionally added chemical species (e.g. volatile organic compounds (VOCs) or NH_3). Uniform ultraviolet (UV) illumination (Kupc et al., 2011) (250–400 nm) emanates from 240 optical fibre vacuum feedthroughs installed on top of the chamber.

For the experiments described here, we formed and grew sulphuric acid particles in the chamber by oxidising SO_2 with OH radicals that were generated by photolysing O_3 and allowing the resulting $\text{O}(^1\text{D})$ to react with water vapour. During these experiments we fed the aerosol population to an array of instruments for characterisation of both physical (mobility) size distribution and composition.



3.1.2 The array of instruments

To sample and analyse the contents of the chamber we utilized the following instruments. Trace gas analysers included an SO₂ monitor (Enhanced Trace Level SO₂ 15 Analyser, Model 43i-TLE, Thermo Scientific, USA), and an O₃ monitor (TEI 49C, Thermo Environmental Instruments, USA). A Chemical Ionisation Mass Spectrometer (CIMS) measured the gas-phase H₂SO₄ concentration ([H₂SO_{4(g)}]) between ~5·10⁵ and ~3·10⁹ cm⁻³ (Kürten et al., 2011; Kürten et al., 2012). The CIMS data provided the total gaseous sulphuric acid concentration, [H₂SO_{4(g)}] without constraining the hydration state of the evaporating molecules (e.g. H₂SO₄ associated with one, or two, or three H₂O molecules).

We measured the evolution of the aerosol number size distribution with a Scanning Mobility Particle Sizer (SMPS, Wang and Flagan, 1990), which recorded the dry particle diameter in the size range from about 10 to 220 nm. We operated the SMPS system with a recirculating dried sheath flow (RH<14 % controlled by a silicon dryer) with a sheath to aerosol sample flow ratio of 3:0.3 L. We maintained the Differential Mobility Analyser (DMA) and recirculating system at 378–388 K by means of a temperature control rack, while we operated the Condensation Particle Counter (CPC) at room temperature. We corrected the SMPS measurements for charging probability, including the possibility of multiple charges, diffusion losses, and CPC detection efficiency.

An Aerodyne Aerosol Mass Spectrometer (AMS) measured aerosol particle chemical composition including sulphate, nitrate, ammonium and organics from particles between 50 and 1000 nm aerodynamic diameter (Jimenez et al., 2003a; Drewnic et al., 2006; Canagaratna et al., 2007). The AMS provided the mass concentration measurements (μg·m⁻³) calculated from the ion signals by using measured air sample flow rate, nitrate ionization efficiency (IE) and relative IE of the other species.

3.2 The experimental procedure

To study aerosol particle evaporation, the formation of sulphuric acid particles preceded. At the lowest H₂O levels (RH<10 %) and in the presence of O₃, controlled UV photo-excitation reactions initiated the oxidation of SO₂ to H₂SO₄. Sulphuric acid particles nucleated and grew to a size of ~220 nm by condensation of H₂SO_{4(g)} at a quasi-constant gas phase concentration (~1·10⁹ cm⁻³ with an uncertainty of >20 %). The H₂SO₄ formation and particle growth ended when we closed the shutters in the front of the UV light source. Afterwards, we induced particle shrinkage by decreasing the RH. We decreased the RH in two separate ways; either by minimizing the influx of water vapour to the chamber, or by increasing the temperature. This separation in experimental procedures gave the ability to achieve and control extremely low RH values (Table 1).

After the end of the particle formation period and during the initial steps of evaporation, before the RH started to decrease, the aerosol size distribution remained nearly constant. Subsequently, the RH decreased gradually initiating the particle evaporation. When the RH reached a certain low value (RH≤1.5 % for T=288.8 K) the particles shrank rapidly, as revealed by the SMPS measurements, and the [H₂SO_{4(g)}] increased until it reached a peak value (Supplement, Fig. S1). The [H₂SO₄]_{peak} was significantly higher than the background concentration before the onset of evaporation (Table 1). After reaching a maximum in gas-phase concentration, the sulphuric acid decreased again, though the size distribution remained



stable (e.g., ~50 (± 10) nm for experiments 1 and 2, see Section 4.3) depending on the RH and T conditions. This behaviour revealed that the remaining aerosol could not be pure sulphuric acid, but rather consisted of a more stable chemical mixture that inhibited further evaporation.

Similarly, the AMS recorded the evaporation of particles (Supplement, Fig. S1). The AMS measurements showed that the particles were composed almost exclusively of sulphuric acid (but not pure H₂SO₄). Based on AMS data, calculations of the kappa value (κ), which is defined as a parameter that describes the aerosols water uptake and cloud condensation nucleous activity (CCN activity), (Petters and Kreidenweis, 2007) of the mixed particles as a function of time during particle formation and evaporation (Supplement, Fig. S2) yield a value close to the κ for pure sulphuric acid particles (Sullivan et al., 2010). A κ value is indicative of the solubility of aerosol particles, with $\kappa=0$ referring to an insoluble particle and $\kappa=0.7$ to pure sulphuric acid particles. κ is computed by the approximate equation

$$\kappa = \frac{4 \cdot A^3}{27 \cdot D_d^3 \cdot \ln^2 S_c}$$

when the critical diameter D_d and critical saturation S_c (or supersaturation, s_c , when referring to CCN activity) are known. The term A can be calculated from the water properties.

3.3 The model framework

In order to understand the processes governing the observed particle evaporation, we modelled the system using the Aerosol Dynamics, gas- and particle-phase chemistry model for laboratory CHAMber studies (ADCHAM, Roldin et al., 2014). ADCHAM includes detailed modules for: (i) aerosol dynamics (coagulation, condensation, deposition and nucleation (nano condensation nuclei formation), (ii) particle-phase chemistry, (iii) mass-transfer limited diffusion in the particle-bulk phase (a kinetic multilayer model), and (iv) gas-phase chemistry based on the Master Chemical Mechanism, MCMv3.3, gas-phase kinetics (Jenkin et al., 1997, 2003; Saunders et al., 2003). ADCHAM has previously been applied to study the mass-transfer limited evaporation of secondary organic aerosol (SOA) particles formed from α -pinene ozonolysis (Roldin et al., 2014) and nano-CN formation and growth from real plant emissions (Roldin et al., 2015).

In the present work we use ADCHAM to study the evolution of the particle number size distribution and particle chemical composition. Instead of simulating the new-particle formation in the CLOUD chamber, we use the measured particle number size distribution before the UV-lights are turned off as well as time sequences of RH, T and [H₂SO_{4(g)}] as inputs to the model (Fig. 1). In order to capture the evolution of the particle number size distribution we consider Brownian coagulation, particle wall deposition, and evaporation of H₂SO₄, SO₃ and H₂O from the particles.

3.3.1 The activity coefficients

Within an aqueous electrolyte solution, such as the H₂SO₄-SO₃-H₂O system, cations, anions and molecular species all disrupt ideality. Here, we consider interactions between ions (HSO₄⁻, SO₄²⁻, NH₄⁺, H⁺), molecules (H₂SO₄, SO₃) and H₂O in the particle-phase chemistry module. To calculate the activity coefficients for the inorganic ions and water we apply the Aerosol



Inorganic Organic Mixtures Functional groups Activity Coefficients (AIOMFAC) model (validated at room temperatures, Zuend et al., 2008 and 2011). AIOMFAC considers interactions between 12 different ions (including HSO_4^- , SO_4^{2-} , NH_4^+ , H^+), water and organic compounds with over 50 UNIFAC-type functional groups (e.g. alcohol, aldehyde, carboxylic acid and hydroperoxides). The reference state for ions and water in the model is an infinitely dilute aqueous solution ($\gamma_i(\chi_{\text{H}_2\text{O}} \rightarrow 1) = 1$, $\gamma_{\text{H}_2\text{O}}(\chi_{\text{H}_2\text{O}} \rightarrow 1) = 1$). γ_i and $\gamma_{\text{H}_2\text{O}}$ are the activity coefficients for the ions (i) and H_2O , respectively.

For relatively dilute $\text{H}_2\text{SO}_{4(\text{aq})}$ solutions (low solute concentration), typical for most atmospheric conditions, it is reasonable to assume that the dissociation of H_2SO_4 to HSO_4^- (R1) is complete (Clegg et al., 1998, Zuend et al., 2008). However, in this work we demonstrate that this assumption fails at low RH and also for small particles with a large Kelvin term. Furthermore, at a very low water activity (a_w) (less than ~ 0.01) a non-negligible fraction of the H_2SO_4 could potentially decompose to SO_3 (R3); if this were the case, the thermodynamic model would need to consider not only R1 but R3 as well (Fig.1).

Since AIOMFAC does not consider inorganic non-electrolyte compounds like H_2SO_4 and SO_3 we implement additionally to this the activity coefficient model symmetric electrolyte–NonRandom Two–Liquid, eNRTL (Bollas et al., 2008, Song and Chen, 2009) which is optimized for the H_2SO_4 – H_2O – SO_3 systems by Que et al., (2011). In this work we use the regressed eNRTL binary interaction parameters from Que et al., 2011. A non-zero interaction parameter is the difference of the dimensionless interaction energies between the electrolyte–molecule pair and the molecule–molecule pair and between the molecule–electrolyte pair and the electrolyte–electrolyte pair (Chen et al., 1982). Binary interaction parameters can also be between molecule–molecule pairs or electrolyte–electrolyte pairs (zero binary parameters). The variation in binary parameter values is a consequence of the strength of the interaction between the different pairs which follow the descending order: electrolyte–electrolyte > molecule–electrolyte > molecule–molecule. Following the convention of the eNRTL model (Chen et al., 1982), we set the unknown binary parameters for NH_4^+ –molecule, molecule– NH_4^+ and NH_4^+ –ions to -4 , 8 and 0 , respectively.

The thermodynamic module provides modelled activity coefficients $\gamma_{\text{H}_2\text{SO}_4}$ and γ_{SO_3} (Fig. S3) as a function of the a_w (Fig. S4.a) and $N:S$, $\chi_{N(\text{III})};\chi_{S(\text{VI})}$. The modelled $\gamma_{\text{H}_2\text{SO}_4}$ and γ_{SO_3} approach unity not only at the standard state of the pure liquids ($\gamma_{\text{H}_2\text{SO}_4}(\chi_{\text{H}_2\text{SO}_4} \rightarrow 1) = 1$ and $\gamma_{\text{SO}_3}(\chi_{\text{SO}_3} \rightarrow 1) = 1$), but also for the infinitely dilute aqueous solution ($\gamma_{\text{H}_2\text{SO}_4}(\chi_{\text{H}_2\text{O}} \rightarrow 1) = 1$ and $\gamma_{\text{SO}_3}(\chi_{\text{H}_2\text{O}} \rightarrow 1) = 1$). This is because the eNRTL binary H_2O – H_2SO_4 and H_2O – SO_3 interaction parameters are zero in the model. For all conditions between these limiting states, the short-range ion (HSO_4^- , SO_4^{2-} , NH_4^+ , H^+) –molecule (H_2SO_4 , SO_3) interactions, and Pitzer–Debye–Hückel long-range ion–molecule interactions influence the modelled $\gamma_{\text{H}_2\text{SO}_4}$ and γ_{SO_3} . At $T = 288.8 \text{ K}$, $\gamma_{\text{H}_2\text{SO}_4}$ reaches the highest values (~ 2.29) when $a_w \approx 0.25$ and γ_{SO_3} reaches the highest values (~ 1.95) when $a_w \approx 0.35$ (Fig. S3). We also assume that the activity coefficient of NH_3 is unity for the model simulations. However, sensitivity tests performed for $\gamma_{\text{NH}_3} = 0.1$ and $\gamma_{\text{NH}_3} = 10$ reveal that, for the acidic particles ($N:S < 1$), our model results are completely insensitive of the absolute value of γ_{NH_3} .



3.3.2 The particle phase composition

If ammonium cation (NH_4^+) is present in the sulphuric acid particles, then solid ammonium bisulfate ($\text{NH}_4\text{HSO}_4(\text{s})$) may form when the S(VI) and H_2O start to evaporate from the particles. However, the particles may also stay as highly supersaturated droplets with respect to the crystalline phase (Zuend et al., 2011). The particle number size distribution measurements do not indicate a sudden drop in particle size, which would be expected if the particles are crystalizing and all particle water is suddenly removed. Thus, in the present work we do not consider any solid salts formation. We further neglect the influence of any mass–transfer limitations in the particle phase, and assume that the particle ion–molecule equilibrium composition (R1–R3) and water content can be modelled as equilibrium processes (because they are established rapidly compared to the composition change induced by the evaporation of H_2SO_4 and SO_3). We use the thermodynamic module to update the particle equilibrium water content, mole fractions and activity coefficients of all species. Then the model considers the gas–particle partitioning of H_2SO_4 and SO_3 with a condensation algorithm in the aerosol dynamics module (Sect. 3.3.5). The time step set in the model is 1s.

The thermodynamic module uses an iterative approach to calculate the particle equilibrium mole fractions of H_2O , H_2SO_4 , SO_3 , HSO_4^- , SO_4^{2-} , NH_3 , NH_4^+ and H^+ , based on the current time step, known RH, and absolute number of moles of S(VI) and N(–III) for each particle size bin. The modelled particle–phase mole fraction of N(–III) during the evaporation experiments is always substantially lower than that of S(VI) ($\text{N}:\text{S}<0.7$). For these particles the saturation vapour pressure of NH_3 is always less than 10^{-10} Pa, within the experimental water activity range 0–0.11 and $\gamma_{\text{NH}_3}\geq 0.1$. Thus, it is reasonable to assume that during the experiments NH_3 does not evaporate from the particles.

Based on the particle diameters from the previous time step (which depend on the particle water content), the thermodynamic module starts by calculating a_w for each particle size, considering the Kelvin effect. Given a_w , the model estimates the particle water mole fraction. Then the model calculates the H^+ molality in the aqueous phase via a 4th order polynomial, derived from the ion balance equation (Eq. 1) in combination with the thermodynamic equilibrium constant equations (Eq. 2–5), and the S(VI) and N(–III) mole balance equation (Eq. 6–7). The maximum positive real root of this polynomial gives the H^+ concentration, $[\text{H}^+]$.

$$[\text{H}^+] + [\text{NH}_4^+] = [\text{HSO}_4^-] + 2[\text{SO}_4^{2-}] \quad (1)$$

$$K_{\text{H}_2\text{SO}_4} = \frac{[\text{HSO}_4^-] \cdot \gamma_{\text{HSO}_4^-} \cdot [\text{H}^+] \cdot \gamma_{\text{H}^+}}{[\text{H}_2\text{SO}_4] \cdot \gamma_{\text{H}_2\text{SO}_4}} \quad (2)$$

$$K_{\text{HSO}_4^-} = \frac{[\text{SO}_4^{2-}] \cdot \gamma_{\text{SO}_4^{2-}} \cdot [\text{H}^+] \cdot \gamma_{\text{H}^+}}{[\text{HSO}_4^-] \cdot \gamma_{\text{HSO}_4^-}} \quad (3)$$

$${}^x K_{\text{SO}_3} = \frac{\chi_{\text{H}_2\text{SO}_4} \cdot \gamma_{\text{H}_2\text{SO}_4}}{\chi_{\text{SO}_3} \cdot \gamma_{\text{SO}_3} \cdot \chi_{\text{H}_2\text{O}} \cdot \gamma_{\text{H}_2\text{O}}} \quad (4)$$



$$K_{NH_3} = \frac{[NH_3] \cdot \gamma_{NH_3} \cdot [H^+] \cdot \gamma_{H^+}}{[NH_4^+] \cdot \gamma_{NH_4^+}} \quad (5)$$

$$n_{S(VI)} = n_{H_2SO_4} + n_{HSO_4^-} + n_{SO_4^{2-}} + n_{SO_3} \quad (6)$$

$$n_{N(-III)} = n_{NH_4^+} + n_{NH_3} \quad (7)$$

The thermodynamic equilibrium coefficients for H_2SO_4 and HSO_4^- dissociation and NH_3 protonation (Eq. 2, 3 and 5) are given in a molality based form while the equilibrium coefficient in Eq. 4, which involves the equilibration between the different solvents (H_2O , SO_3 and H_2SO_4), is given in a mole–fraction based form. The model calculates $K_{HSO_4^-}$ and K_{NH_3} ($\text{mol} \cdot \text{kg}^{-1}$) with Eq. 8 and 9 (Jacobson, 2005a). We treat $K_{H_2SO_4}$ and ${}^xK_{SO_3}$ as unknown model fitting parameters.

$$K_{HSO_4^-} = 1.015 \cdot 10^{-2} \cdot e^{\left(8.85 \cdot \left(\frac{298}{T} - 1\right) + 25.14 \cdot \left(1 + \ln\left(\frac{298}{T}\right) - \frac{298}{T}\right)\right)} \quad (8)$$

$$K_{NH_3} = 1.7882 \cdot 10^9 \cdot e^{21.02 \cdot \left(\frac{298}{T} - 1\right)} \quad (9)$$

Once $[H^+]$ is determined, all other ion and molecule concentrations can be derived from Eq. 1–7. Based on the new estimated particle–phase ion and molecule mole fractions, the thermodynamic module uses AIOMFAC and eNRTL to update the ion and molecule activity coefficients. The model then repeats the whole procedure iteratively until the relative change in the concentration and activity coefficients for each compound is less than 10^{-9} between successive iteration steps. To stabilize convergence, the model estimates activity coefficients used in the proceeding iteration as a weighted average of the values from the previous and present iteration time steps.

3.3.3 H_2SO_4 and SO_3 in the gas–phase

In the gas phase only a fraction of H_2SO_4 is in the form of pure sulphuric acid molecules while the rest of the H_2SO_4 is in a hydrated form. In this work we use the parameterization from Hanson and Eisele (2000), who measured the diffusion loss rate of H_2SO_4 to flow–tube walls at different RH, to estimate the RH–dependent effective diffusion coefficient of $H_2SO_4(g)$.

In the gas phase, SO_3 reacts rapidly with H_2O to form H_2SO_4 . Based on the measured loss rate of SO_3 , which shows a second–order dependence on the water vapour concentration (Jayne et al., 1997), we estimate that $SO_3(g)$ is converted to $H_2SO_4(g)$ in less than 1s during the CLOUD chamber experiments, even at the lowest RH. Because of this rapid conversion to H_2SO_4 and the high vapour pressure of SO_3 (Eq. 11), it is reasonable to assume that the gas–phase concentration of SO_3 (vapour pressure, $p_{\infty, SO_3(g)}$) is negligibly low.



3.3.4 Saturation vapour pressures, surface tension and particle density

We use Eq. 10 and 11 to calculate the temperature dependent sub-cooled pure-liquid saturation vapour pressures for H₂SO₄ and SO₃ ($p_{0,i}$, where i refers to H₂SO₄ or SO₃ in Pa). Equation 10 is based on the work of Ayers et al. (1980), with corrections for lower temperatures by Kulmala and Laaksonen (1990). We use the (best fit) L parameter value of -11.695 (Noppel et al., 2002, Noppel–Kulmala–Laaksonen, N–K–L, parameterisation, (Supplement Fig.S5.a)). Equation 11 is based on the work of Nickless (1968) (Supplement Fig.S5.b)).

$$p_{0,H_2SO_4} = 101325 \cdot e^{\left(L+10156 \left[\frac{1}{360.15} - \frac{1}{T} + \frac{0.38}{545} \left(1 + \ln \left(\frac{360.15}{T} \right) - \frac{360.15}{T} \right) \right] \right)} \quad (10)$$

$$p_{0,SO_3} = e^{\left(\frac{28.9239 - \frac{7000}{T}}{133.3224} \right)} \quad (11)$$

As an alternative to Eq. 10 and 11 we also use the H₂SO₄ and SO₃ pure-liquid saturation vapour pressure parameterisations from Que et al., 2011 (originally from the Aspen Plus Databank) (Fig. S5).

We calculate the saturation vapour pressures of H₂SO₄ and SO₃ for each particle size with Eq. 12, using the mole fractions ($\chi_{i,j}$) and activity coefficients ($\gamma_{i,j}$) of H₂SO₄ and SO₃ (from the thermodynamic model) and the Kelvin term ($C_{k,i,j}$ Eq. 13) for compound i in particle size bin j .

$$p_{s,i,j} = p_{0,i} \cdot a_{i,j} \cdot C_{k,i,j} \quad (12)$$

where $a_{i,j} = \chi_{i,j} \cdot \gamma_{i,j}$

$$C_{k,i,j} = e^{\left(\frac{4M_i\sigma_j}{RT\rho_{p,j}D_{p,j}} \right)} \quad (13)$$

$a_{i,j}$ is the activity of compound i in size bin j , T is the temperature in Kelvin, R is the universal gas constant ($J \cdot mol^{-1} \cdot K^{-1}$), M_i is the molar mass ($kg \cdot mol^{-1}$) of compound i , $\rho_{p,j}$ is the density ($kg \cdot m^{-3}$) of the liquid particles, σ_j is the surface tension ($N \cdot m^{-1}$) and $D_{p,j}$ is the particle diameter (m) of the particles in size bin j .

As an alternative approach we also model the evaporation of H₂SO₄ using composition dependent H₂SO₄ activities ($a_{H_2SO_4,j}$) derived directly from the tabulated values of the difference in chemical potentials between the sulphuric acid in aqueous solution and that of the pure acid ($\mu_{H_2SO_4,j} - \mu_{H_2SO_4}^0$). The tabulated values that are valid at 298.15 K are taken from Giauque et al. (1960). The relationship between $\mu_{H_2SO_4,j} - \mu_{H_2SO_4}^0$ and $a_{H_2SO_4,j}$ is given by Eq. 14.

$$\ln(a_{H_2SO_4,j}) = (\mu_{H_2SO_4,j} - \mu_{H_2SO_4}^0) / (R \cdot T) \quad (14)$$



In accordance with Ayers et al. (1980) we neglect any temperature dependence of $\mu_{H_2SO_4,j} - \mu_{H_2SO_4}^0$. This empirically based approach is used in several chemistry transport models to simulate the evaporation of pure sulphuric acid particle in the stratosphere (see e.g. Kokkola et al., 2009 and Hommel et al., 2011).

We calculate the surface tension and density of the particles comprising a ternary mixture of water, sulphuric acid and ammonium with parameterisations given by Hyvärinen et al. (2005) that combine surface tension parameterisations (measurements) for $(NH_4)_2SO_4-H_2O$ mixtures (Hämeri et al., 2000, Korhonen et al., 1998b), $H_2SO_4-H_2O$ mixtures (Vehkamäki et al., 2002) and NH_3-H_2O mixtures (King et al. 1930). For the range of conditions in our experiment, where the minimum particle diameter after evaporation is $\sim 50(\pm 10)$ nm (for experiments 1 and 2). The Kelvin effect only increases the water saturation vapour pressure by maximum value of 1.07 (and the H_2SO_4 saturation vapour pressure by 1.44, Supplement Fig. S6) for the particle diameter of 40 nm (exp.2).

3.3.5 Evaporation of H_2SO_4 , SO_3 and H_2O

We model the gas–particle partitioning (evaporation) of H_2SO_4 and SO_3 using the full moving size distribution method in combination with the Analytic Prediction of Condensation, APC scheme (Jacobson, 2005a). APC is an unconditionally stable numerical discretisation scheme used to solve the condensation equation (Eq. 15). In Eq. 15, we substitute the saturation vapour pressures from Eq.12 and the measured concentration, $C_{\infty,H_2SO_4(g)}$, (vapour pressure, $p_{\infty,H_2SO_4(g)}$) of $H_2SO_4(g)$. Based on the motivation given in Sect. 3.3.3 the vapour pressure of SO_3 , $p_{\infty,SO_3(g)}$, is set to zero.

$$\frac{dm_{i,j}}{dt} = \frac{2 \cdot \pi \cdot (d_i + d_j) \cdot (D_i + D_j) \cdot M_i}{R \cdot T} \cdot f_{i,j}(Kn_{i,j}, \alpha_i) \cdot (p_{\infty,i} - p_{s,i,j}) \quad (15)$$

$$f_{i,j}(Kn_{i,j}, \alpha_i) = \frac{Kn_{i,j} + 1}{0.377 \cdot Kn_{i,j} + 1 + \frac{4}{3 \cdot \alpha_i} \cdot (Kn_{i,j}^2 + Kn_{i,j})}$$

$$Kn_{i,j} = \frac{2 \cdot \lambda_{i,j}}{d_i + d_j}, \quad \lambda_{i,j} = \frac{3 \cdot (D_i + D_j)}{\sqrt{v_i^2 + v_j^2}} \quad (16)$$

Equation 15 describes the contribution of species i to the mass growth rate of a particle in size bin j , $f_{i,j}$ is the Fuchs–Sutugin correction factor in the transition region (Fuchs and Sutugin, 1971), d_i, d_j correspond to diameters (m) and D_i, D_j to diffusion coefficients ($m^2 \cdot s^{-1}$) of the condensing molecule i and the particles in size bin j , respectively. α_i is the mass–accommodation coefficient of compounds i and $Kn_{i,j}$ is the non–dimensional Knudsen number (Eq.16). $\lambda_{i,j}$ is the mean free path (m) and v_i, v_j are the thermal speed ($m \cdot s^{-1}$) of the molecule i and the particles in size bin j , respectively. Equations 15 and 16 take into account that the condensing molecules have a non–negligible size compared to the size of the smallest particles, and that small particles have non–negligible diffusion coefficients (Lehtinen and Kulmala, 2003).



Based on measurements of H_2SO_4 losses in a flow tube reactor, Pöschl et al., (1998) derived a mass accommodation coefficient of $\text{H}_2\text{SO}_4(\text{g})$ on aqueous sulphuric acid, $\alpha_{\text{H}_2\text{SO}_4}$, which was close to unity, with a best fit value of 0.65, a lower limit value of 0.43 and an upper limit of 1.38 (physical limit 1.0). The measured mass accommodation coefficients did not show any dependence on the relative amount of water in the particles (Pöschl et al., 1998). For the model simulations in this work we use unity mass accommodation coefficients. The particle water content is modelled as an equilibrium process with the thermodynamic module (see Sect. 3.3.2).

3.3.6 Particle losses

A detailed description of how ADCHAM treats particle wall deposition losses is given in Roldin et al. (2014). Here we only describe the specific assumptions made for the model simulations performed in this study.

The electric field strength of the stainless-steel CLOUD chamber, in contrast to smog chambers made of Teflon, is very low. Therefore we can neglect electrostatic deposition enhancements. We simulate the particle size-dependent deposition losses with the model from Lai and Nazaroff (2000), which considers the area of vertical, upward, and downward facing horizontal chamber wall surfaces. The particle deposition loss depends on the friction velocity (u^*), which we treat as an unknown model fitting parameter. The best possible agreement between the modelled and measured particle number and volume concentration in the chamber is achieved with a friction velocity of $\sim 0.2 \text{ m}\cdot\text{s}^{-1}$. Thus, for all model results we present in this article we use $u^* = 0.2 \text{ m}\cdot\text{s}^{-1}$.

Dilution losses due to the purified air injected to the CLOUD chamber are also considered in the model.

3.3.7 Constraining the thermodynamic properties of sulphate aerosol particles

We use ADCHAM to constrain the values of the thermodynamic equilibrium coefficients, $K_{\text{H}_2\text{SO}_4}$ and ${}^xK_{\text{SO}_3}$, by treating these coefficients as unknown model fitting parameters. By varying the equilibrium coefficients we search for the best possible agreement (coefficient of determination (R^2), see Table 2.) between the modelled and measured Geometric Mean Diameter (GMD) with respect to particle number. Because experimental results reveal that the sulphate particles did not evaporate completely, they must have been contaminated with a small fraction of effectively non-volatile material (Sect. 3.2).

In the model we address this by assuming that the particles (prior to evaporation) contained either a small fraction of non-volatile organic material (e.g., secondary organic aerosol, SOA) or that the particles contained small amounts of ammonium, which prevented H_2SO_4 formation and consequently evaporation. We calculate the initial SOA and ammonium dry particle volume fraction in particle size bin j ($\chi^{\text{v}_{\text{SOA},j}}$ and $\chi^{\text{v}_{\text{NH}_4^+,j}}$) with Eq. 17 and 18, respectively. Here d_{SOA} and $d_{\text{NH}_4^+}$ represent an effective particle diameter of SOA and ammonium if all other particle species are removed. For experiment 1 we use $d_{\text{SOA}} = 60 \text{ nm}$ and $d_{\text{NH}_4^+} = 26 \text{ nm}$, for experiment 2 $d_{\text{SOA}} = 43 \text{ nm}$ and $d_{\text{NH}_4^+} = 19 \text{ nm}$ and for experiment 3 $d_{\text{SOA}} = 38 \text{ nm}$ and $d_{\text{NH}_4^+} = 17 \text{ nm}$.



$$\chi_{SOA,j}^v = \min\left(\frac{d_{SOA}^3}{d_j^3}, 0.2\right) \quad (17)$$

$$\chi_{NH_4^+,j}^v = \min\left(\frac{d_{NH_4^+}^3}{d_j^3}, 0.05\right) \quad (18)$$

4 Results and discussion

In order to fit the modelled particle number size distribution evolution to the observations we performed several hundred simulations where we varied $K_{H_2SO_4}$ and ${}^xK_{SO_3}$. We summarize these simulations into three main categories (Cases):

- 1) only H_2SO_4 and H_2O evaporation (${}^xK_{SO_3}=\infty$), (Case 1)
- 2) combination of H_2SO_4 , H_2O and SO_3 evaporation, (Case 2) and
- 3) practically only SO_3 and H_2O evaporation, (Case 3).

Case 2 is further divided into two subcategories, Case 2a and 2b. In Case 2a the H_2SO_4 is the dominant evaporating S(VI) species while in Case 2b the SO_3 is the dominant evaporating S(VI) species.

4.1 Particle–phase mole fractions

Figure 2 shows an example of the modelled mole fractions of (a) $H_2SO_{4(aq)}$, $\chi_{H_2SO_4}$, and (b) $SO_{3(aq)}$, χ_{SO_3} , as a function of the a_w and $N:S$ for Case 2a with equilibrium constants $K_{H_2SO_4}=2.40\cdot 10^9 \text{ mol}\cdot\text{kg}^{-1}$, and ${}^xK_{SO_3}=1.43\cdot 10^{10}$ at $T=288.8 \text{ K}$. Fig. 2 reveals that the increase of χ_{SO_3} as a_w decreases is steeper than for $\chi_{H_2SO_4}$. This is because $H_2SO_{4(aq)}$ formation precedes SO_3 formation (see R3). As expected, the highest values of $\chi_{H_2SO_4}$ and χ_{SO_3} occur when $N:S=0$ and a_w approaches zero. While $N:S$ increases, $\chi_{H_2SO_4}$ and χ_{SO_3} decrease gradually and reach very low values when $N:S$ become larger than 0.6.

4.2 Particle number size distribution evolution

In Figure 3 we present the particle number size distribution evolution after the shutter of the UV light was closed and the influx of water vapour to the chamber was interrupted for experiment 2, performed at $T=288.8 \text{ K}$, showing (a) the measured and (b) the modelled values for Case 2a with $K_{H_2SO_4}=2.40\cdot 10^9 \text{ mol}\cdot\text{kg}^{-1}$ and ${}^xK_{SO_3}=1.43\cdot 10^{10}$. At the beginning of the evaporation process the particles in the size range from ~ 60 to $\sim 180 \text{ nm}$ in diameter contained approximately 70 mole % H_2O ; however, this percentage decreased, declining to 15 mole % (Fig 3c) after 6 hours. Before H_2SO_4 and SO_3 started to evaporate from the particles the assumed mole fraction of ammonium was very low (Fig. 3d). However, during the evaporation process $N:S$ increased steadily until it reached a value of ~ 0.6 after $\sim 6\text{h}$. At this point the particles were $\sim 40 \text{ nm}$ in diameter and did not shrink further. This model result is in good agreement with the experimental results reported by Marti et al. (1997) and confirms that NH_4^+ effectively stabilizes sulphur particles against evaporation when $N:S>0.6$.



4.3 Geometric mean diameter shrinkage influenced by RH

Figure 4 compares the measured and modelled GMD evolution as a function of (a) time and (b) RH for experiments 1 and 2 performed at a temperature of $T=288.8\text{ K}$ (Table 1) with NH_3 as a particle phase contaminant. The model results are from simulations 1–4 and 13–16 listed in Table 2. The pure liquid saturation vapour pressures of H_2SO_4 and SO_3 were calculated with Eq. 10 and 11. The model results are in good agreement with the measured GMD trend for Case 1 ($K_{\text{H}_2\text{SO}_4}=2.00\cdot 10^9\text{ mol}\cdot\text{kg}^{-1}$), Case 2a ($K_{\text{H}_2\text{SO}_4}=2.40\cdot 10^9\text{ mol}\cdot\text{kg}^{-1}$ and ${}^xK_{\text{SO}_3}=1.43\cdot 10^{10}$), Case 2b ($K_{\text{H}_2\text{SO}_4}=4.00\cdot 10^9\text{ mol}\cdot\text{kg}^{-1}$ and ${}^xK_{\text{SO}_3}=1.54\cdot 10^9$) and Case 3 ($K_{\text{H}_2\text{SO}_4}=1.00\cdot 10^{11}\text{ mol}\cdot\text{kg}^{-1}$ and ${}^xK_{\text{SO}_3}=3.33\cdot 10^7$). The Case 3 simulations give a particle shrinkage that begins somewhat too late and occurs somewhat too rapidly. However, considering the measurement uncertainties it is impossible to constrain the relative contribution of H_2SO_4 and SO_3 to the observed GMD loss only based on these two experiments (see Section 4.4).

With the Aspen Plus Databank pure liquid saturation vapour pressure parameterisations it is also possible to find similarly good agreement between the modelled and observed GMD evolution during experiment 1 and 2 for Cases 1–3 (Fig. S8) for NH_3 as a particle phase contaminant, but with somewhat different values of $K_{\text{H}_2\text{SO}_4}$ and ${}^xK_{\text{SO}_3}$ (see Table 2, simulations 8–11 and 20–23).

The model simulations with non-volatile and non-water-soluble organics or dimethylamine (DMA) as the particle phase contaminant gave nearly identical results as with NH_3 , both for experiments 1 and 2 (simulations 6, 7, 17 and 18 in Table 2). In the case of DMA this occurs because NH_3 is also a strong enough base to be completely protonated (all N(–III) is in the form of NH_4^+). In the case of an organic contaminant instead of NH_3 the model results mainly differ at a later stage of the particle evaporation phase when the N:S approaches ~ 0.5 . This is because the evaporation rate does not slow down before all S(VI) is lost if the particles do not contain any base (see Fig. S9). Thus, the modelled GMD shrinkage becomes somewhat faster, when assumed organic contamination. Without any particle phase contamination (pure sulphuric acid particles) the particles evaporate from the very early stage faster and completely (supplement, Fig. S10).

Instead of explicitly calculating the H_2SO_4 activity with the thermodynamics module we also conducted a simulation in which we derived it directly from the tabulated values of the H_2SO_4 chemical potentials as a function of the molality, following Giauque et al. (1960) (Eq. 14). With this method it is possible to simulate the evaporation of H_2SO_4 without explicitly calculating the concentration of H_2SO_4 in the particles. However, since the tabulated chemical potentials from Giauque et al. (1960) is only valid for pure sulphuric acid solutions and temperatures close to 298.15 K it cannot be used if the particle aqueous phase also contains ammonium or other stabilizing molecules.

Figure 5 compares the modelled and measured GMD evolution for experiments 1 and 2 (performed at $T=288.8\text{ K}$) when we use the data from Giauque et al. (1960) and Eq. 14 to derive the H_2SO_4 activity. H_2SO_4 was assumed to be the only evaporating S(VI) species (Case 1), the particle phase contamination consisted of non-volatile non-water-soluble organics, and the pure-liquid saturation vapour pressure of H_2SO_4 was calculated with Eq. 10 or with the Aspen Plus Databank parameterization (simulations 5, 12, 19 and 24 in Table 2). The modelled GMD shrinkage agrees very well with the



observations from experiments 1 and 2 when we use the tabulated H₂SO₄ chemical potential from Giauque *et al.* (1960) in combination with the pure–liquid saturation vapour pressure parameterization from N–K–L parameterisation (Noppel *et al.*, 2002; Kulmala and Laaksonen, 1990) (Eq. 10). However, when we use the pure–liquid saturation vapour pressure parameterisation from the Aspen Plus Databank, the modelled particles evaporate earlier (at higher RH) than the observed particles. This due to ASPEN parameterisation which gives higher saturation vapour pressures compared to N–K–L.

4.4 Geometric mean diameter shrinkage influenced by relative humidity and temperature

In an attempt to constrain how $K_{H_2SO_4}$ and ${}^xK_{SO_3}$ depend on the temperature, and the role of H₂SO₄ and SO₃ on the observed particle diameter shrinkage, as a next step we simulate experiment 3, which expands in temperature. For this experiment the temperature increases gradually from 268 K to 293 K while the absolute humidity remains at a constant value, thus allowing the RH to decrease. Equation 19 describes the modelled temperature dependence of $K_{H_2SO_4}$ and ${}^xK_{SO_3}$ where the K_i values at $T=288.8\text{ K}$ ($K_{i,288.8\text{ K}}$) set equal to the values derived regarding the model simulations of experiment 1 and 2 (Sect. 4.2):

$$K_i = K_{i,288.8\text{ K}} \cdot e^{\left(B_i \left(\frac{1}{T} - \frac{1}{288.8} \right) \right)} \quad (19)$$

where i can be either H₂SO₄ or SO₃. With $B_i=0\text{ K}$ there is no temperature dependence of K_i .

For other acids like HNO₃, HCl and HSO₄[−], K_i decreases with increasing T ($B_i>0$) (Jacobson, 2005a). Que *et al.* (2011) estimated $B_{H_2SO_4}$ to be 3475 K and B_{SO_3} to be −14245.7 K. Thus, based on this information we would expect the equilibrium reactions R1 and R3 to shift towards the left (more H₂SO_{4(aq)} and SO₃ as temperature increases). This would result in a stronger temperature dependence of the H₂SO_{4(aq)} and SO₃ saturation vapour pressures over aqueous sulphuric acid droplets (Eq. 12) compared to the temperature dependence expected if only the temperature effect of the pure–liquid saturation vapour pressures was considered (Fig. S5).

Figure 6 compares the modelled and measured GMD evolution during experiment 3 for simulations where we use either the same temperature dependence as suggested by Que *et al.* (2011) ($B_{H_2SO_4}=3475\text{ K}$ and $B_{SO_3}=-14245.7\text{ K}$), no temperature dependence of $K_{H_2SO_4}$ and ${}^xK_{SO_3}$ ($B_{H_2SO_4}=0\text{ K}$ and $B_{SO_3}=0\text{ K}$) or $B_{H_2SO_4}=0\text{ K}$ and $B_{SO_3}=-3000\text{ K}$. For the case with $B_{H_2SO_4}=0\text{ K}$ and $B_{SO_3}=0\text{ K}$ the model results are given both for a simulation where the particle contamination is assumed to be NH₃ and a simulation where it is treated as non–volatile and non–water–soluble organics. The H₂SO₄ and SO₃ pure liquid saturation vapour pressures are calculated with Eq. 10 and 11. The simulations are listed as number 28, 29, 33, 34 and 36 in Table 2. All simulations except number 28 correspond to scenario Case 2a. In simulation 28 (Case 1) we use Eq. 14 and the tabulated H₂SO₄ chemical potentials from Giauque *et al.* (1960) to derive the H₂SO₄ activity. The model cannot capture the observed GMD evolution if the temperature dependences of $K_{H_2SO_4}$ and ${}^xK_{SO_3}$ are described by the $B_{H_2SO_4}$ and B_{SO_3} values derived by Que *et al.* (2011). Instead the model simulations indicate that the temperature dependences of $K_{H_2SO_4}$ and ${}^xK_{SO_3}$ need to be very weak or insignificant ($B_{H_2SO_4}=0\text{ K}$ and $B_{SO_3}=0\text{ K}$). If the particles are contaminated with NH₃, B_{SO_3} or $B_{H_2SO_4}$ even needs to be negative for optimum fitting (e.g. $B_{H_2SO_4}=0\text{ K}$ and $B_{SO_3}=-3000\text{ K}$). It is also possible to find good agreement between the modelled and measured GMD evolution if one of $B_{H_2SO_4}$ and B_{SO_3} is negative and the other one is positive (see e.g.



Case 2a simulation number 31 in Table 2). For the Case 1 simulation where we used Eq. 14 and the tabulated chemical potentials from Giauque et al. (1960), the modelled particles grow somewhat too much before they start to shrink.

If we instead use the pure-liquid saturation vapour pressure parameterizations from the Aspen Plus Databank (which have somewhat weaker temperature dependences than Eq. 10 and 11), the model results captures the observed GMD evolution if both $B_{\text{H}_2\text{SO}_4}$ and B_{SO_3} are zero and H_2SO_4 is the only evaporating (SVI) species (Case 1, simulations 50 listed in Table 2) or the main evaporating S(VI) species (Case 2a, simulations 51 listed in Table 2) (Fig. 7).

Figure 7 also shows the results from one Case 2b and one Case 3 simulation where both $B_{\text{H}_2\text{SO}_4}$ and B_{SO_3} were set equal to 0 K (simulations 52 and 53 listed in Table 2). However, for these scenarios in which we assume that SO_3 is responsible for most of the S(VI) evaporation, the model can never capture the observed GMD evolution. This is the case regardless of the pure liquid saturation vapour pressure method we use (N-K-L-Nickless or Aspen Plus Databank) or the temperature dependence we assign to $K_{\text{H}_2\text{SO}_4}$ and ${}^xK_{\text{SO}_3}$.

Based on the simulations of experiment 3 we conclude that most of the S(VI) that evaporated from the particles probably was in the form of H_2SO_4 (Cases 1 and 2a). The very weak temperature dependences for $K_{\text{H}_2\text{SO}_4}$ and ${}^xK_{\text{SO}_3}$ needed for the model to capture the GMD evolution during experiment 3 is surprising and calls for further investigation. Part of the explanation to this could be that the AIOMFAC activity coefficient model has been developed based on experimental data derived at 298.15 K. The uncertainty arising from the two different pure liquid saturation vapour pressure parameterisations (temperature dependent) also limits our ability to fully constrain the $K_{\text{H}_2\text{SO}_4}$ and ${}^xK_{\text{SO}_3}$ values. Based on our experiments and model simulations the equilibrium constant $K_{\text{H}_2\text{SO}_4}$ should be somewhere in the range $2.0\text{--}4.0 \cdot 10^9 \text{ mol}\cdot\text{kg}^{-1}$ and the ${}^xK_{\text{SO}_3}$ needs to be larger than $1.4 \cdot 10^{10}$ at a temperature of $288.8 \pm 5 \text{ K}$. The type of contamination of the sulphate particles (NH_3 , DMA or a non-volatile non-water-soluble organic compound) does not have a substantial impact on our results and conclusions.

4.5 Atmospheric implications

From Sect. 4.3 and 4.4 we conclude that the relative contribution of H_2SO_4 and SO_3 to the observed particle volume loss remains uncertain. However, based on the assumption of rapid conversion of $\text{SO}_3(\text{g})$ to $\text{H}_2\text{SO}_4(\text{g})$, we can define an effective saturation concentration of $\text{H}_2\text{SO}_4(\text{g})$ ($C_{\text{H}_2\text{SO}_4,\text{S}}^*$) as the sum of the saturation concentration of H_2SO_4 ($C_{\text{H}_2\text{SO}_4,\text{S}}$) and SO_3 ($C_{\text{SO}_3,\text{S}}$) (Eq. 20).

$$C_{\text{H}_2\text{SO}_4,\text{S}}^* = C_{\text{H}_2\text{SO}_4,\text{S}} + C_{\text{SO}_3,\text{S}} \quad (20)$$

Figure 8 shows the modelled effective H_2SO_4 saturation concentration ($C_{\text{H}_2\text{SO}_4,\text{S}}^*$) as a function of particle size ($d_p = 1\text{--}10^3 \text{ nm}$) and RH (0–100 %). The results are from a model simulation with $K_{\text{H}_2\text{SO}_4} = 2.40 \cdot 10^9 \text{ mol}\cdot\text{kg}^{-1}$ and ${}^xK_{\text{SO}_3} = 1.43 \cdot 10^{10}$, $T = 288.8 \text{ K}$ and pure liquid saturation vapour pressures calculated with Eq. 10 and 11. The four different panels (a–d) correspond to simulations using four different values for N:S, namely 0, 0.5, 0.75 and 1. In each panel, the contours show the $\log_{10}(C_{\text{H}_2\text{SO}_4,\text{S}}^*)$ levels. For example, the $\log_{10}(C_{\text{H}_2\text{SO}_4,\text{S}}^*) = 7$ contour corresponds to an effective H_2SO_4 saturation concentration of 10^7 molecules



cm⁻³. These contours provide the H₂SO₄ gas-phase concentration at which the net flux of S(VI) to and from the particles is zero (particles neither grow nor shrink).

The observed atmospheric daytime range of the gas-phase H₂SO₄ concentration is approximately 10⁵–10⁸ molecules cm⁻³, and so we shade this range in Figure 8. When $C^*_{H_2SO_4,S}$ is less than this range (to the upper right in the panel), the particles for most atmospheric daytime conditions will grow by condensation of H₂SO₄; when $C^*_{H_2SO_4,S}$ is greater than this (to the lower left in the panel) the particles will for most conditions shrink by evaporation of S(VI); in the shaded range the particles will tend to equilibrate. The larger the mole fraction of bases (NH₃) in the aerosol particles the less prone they will be to shrink. When particles are composed only of S(VI) and H₂O ($N:S=0$) and the concentration of H₂SO_{4(g)} is 10⁷ molecules cm⁻³ all particles smaller than 10 nm will shrink at $RH < 13.2\%$. For the same H₂SO_{4(g)} concentration and $N:S=0.5$ all particles smaller than 10 nm shrink at $RH < 12.1\%$. However, for $N:S=0.75$ particles smaller than 4 nm shrink at $RH < 5.5\%$, and if $N:S=1$ only particles smaller than ~1.9 nm shrink, independent of RH except when it is extremely dry ($RH \leq 1.5\%$). With the vapour pressure parameterisations from the Aspen Plus Databank and $K_{H_2SO_4}=4.00 \cdot 10^9$ and ${}^xK_{SO_3}=4.55 \cdot 10^{10}$ the results are nearly identical.

5 Summary and conclusions

At low relative humidity ($RH \lesssim 1.5\%$), the dissociation of H₂SO_{4(aq)} is not complete, and evaporation of H₂SO₄ and H₂O can explain the particle shrinkage we observe in the CLOUD chamber at CERN. Some of the evaporating S(VI) may also be, in some extent, SO₃ formed from dehydration of H₂SO_{4(aq)}. The equilibrium rate coefficient for the first dissociation stage of H₂SO_{4(aq)} ($K_{H_2SO_4}$) falls somewhere in the range $2.0\text{--}4.0 \cdot 10^9 \text{ mol}\cdot\text{kg}^{-1}$ at 288.8 ± 5 K. The equilibrium coefficient for the dehydration of H₂SO₄ (${}^xK_{SO_3}$) is larger than $1.4 \cdot 10^{10}$. The main factors limiting our estimation of $K_{H_2SO_4}$ are uncertainties in (i) the pure liquid saturation vapour pressure of H₂SO₄ and (ii) the relative contribution of SO₃ to the observed particle evaporation. Other potential sources of error are the uncertainties in the derived activity coefficients, the mass accommodation coefficient of H₂SO₄ and solid salt formation during the particle evaporation phase. Based on the model simulations of an experiment where the temperature was gradually increased from 268 to 293 K, the temperature dependencies of $K_{H_2SO_4}$ and ${}^xK_{SO_3}$ need to be weak. Future studies should focus on constraining the pure liquid saturation vapour pressures of H₂SO₄ and SO₃.

Our results are meaningful for atmospheric processes such as new-particle formation occurring in free troposphere and stratosphere. The equilibrium constants of formation and dissociation of H₂SO₄ reported in this study provide a tool to model the excess H₂SO₄ responsible for the gas-to-particle conversion. Furthermore, in the ternary system H₂SO₄–NH₃–H₂O the dissociation of H₂SO₄ influences the H⁺ concentration in sulphur aerosol particles (eq.R1 and R2) that affect the solubility of NH₃. Moreover, vapour-phase H₂SO₄ in the atmosphere appears to be ubiquitous, even in the absence of photochemistry (Mauldin et al. 2003; Wang et al., 2013); this may partly be due to evaporation of H₂SO₄ from aerosol particles. In a changing climate it will become even more important to understand the thermodynamic properties of the sulphur aerosol particles involved in the development of polar stratospheric clouds and how sulphate aerosols influence the stratospheric O₃ layer.



Experiments simulating stratospheric conditions ($T \approx 200\text{--}265\text{ K}$, $p \approx 10^{-1}\text{--}10^{-3}\text{ atm}$, $RH \geq 1.0\%$ and $[H_2SO_4] \leq 10^8\text{ molec. cm}^{-3}$), are also of great importance. Our results may also assist in explaining the atmospheric sulphur cycle of Venus. The Venusian clouds made up largely of sulfuric acid droplets cover an extended temperature range from 260 K (upper clouds) to 310 K (middle clouds) and even higher (lower clouds). Under such conditions there is a need for similar studies at higher temperatures
5 than the range covered in this study.

10

15

20

25

30



Author Contributions

G.T. and J.D. designed and performed the experiments. G.T., J.D. and P.R. analysed the data. P.R. developed the model code. P.R. and G.T. optimized the model and performed the simulations. G.T., J. D., L. R., J. T., J. G. S., and A.K. collected the data and contributed to the analysis. G.T, P.R., and N.M.D assisted in drafting the manuscript. G.T., P. R., J. D., M. B., J. C., R. C. F., M. K., N. M. D., F. S. contributed to scientific interpretation and editing of manuscript. All authors contributed to the development of the CLOUD facility and analysis instruments, and commented on the manuscript.

Data availability

Requests for underlying material should be addressed to the corresponding author G.T (george.tsagkogeorgas@tropos.de).

Acknowledgements

10 We would like to thank CERN for supporting CLOUD with important technical and financial resources, and for providing a particle beam from the CERN Proton Synchrotron. We also thank P. Carrie, L.–P. De Menezes, J. Dumollard, R. Guida, K. Ivanova, F. Josa, I. Krasin, R. Kristic, A. Laassiri, O.S. Maksumov, S. Mathot, B. Marichy, H. Martinati, S.V. Mizin, A. Onnela, R. Sitals, H.U. Walther, A. Wasem and M. Wilhelmsson for their important contributions to the experiment. This research has received funding from the EC Seventh Framework Programme (Marie Curie Initial Training Network “CLOUD–
15 ITN” no. 215072 and “CLOUD–TRAIN” no. 316662, ERC–Starting “MOCAPAF” grant no. 57360 and ERC–Advanced “ATMNUCLE” grant no. 227463), the German Federal Ministry of Education and Research (project nos. 01LK0902A and 01LK1222A), the Swiss National Science Foundation (project nos. 200020 135307 and 206620 141278), the Academy of Finland (Center of Excellence project no. 1118615 and other projects 135054, 133872, 251427, 139656, 139995, 137749, 141217, 141451), the Finnish Funding Agency for Technology and Innovation, the Vaisala Foundation, the Nessling
20 Foundation, the Austrian Science Fund (FWF; project no. J3198–N21), the Portuguese Foundation for Science and Technology (project no. CERN/FP/116387/2010), the Swedish Research Council, Vetenskapsradet (grant 2011–5120), the Presidium of the Russian Academy of Sciences and Russian Foundation for Basic Research (grants 08–02–91006–CERN and 12–02–91522–CERN), the U.S. National Science Foundation (grants AGS1136479, AGS1447056, AGC1439551 and CHE1012293), the PEGASOS project funded by the European Commission under the Framework Program 7 (FP7–ENV–2010–265148), and
25 the Davidow Foundation. We thank the tofTools team for providing tools for mass spectrometry analysis.
P. Roldin would like to thank the Cryosphere–Atmosphere Interactions in a Changing Arctic Climate (CRAICC) and the Swedish Research Council for Environment, Agricultural Sciences and Spatial Planning FORMAS (Project no. 214–2014–1445) for financial support.



References

- Abbatt, J. P. D. and Nowack, J. B.: Heterogeneous interactions of HBr and HOCl with cold sulfuric acid solutions: implications for Arctic boundary layer bromine chemistry, *J. Phys. Chem. A*, 101, 2131–2137, 1997.
- Acosta Navarro, J. C., Varma, V., Riipinen, I., Seland, Ø., Kirkevåg, A., Struthers, H., Iversen, T., Hansson, H. – C. and Ekman, A. M. L.: Amplification of Arctic warming by past air pollution reductions in Europe, *Nature Geos.* 9, 277–281, 2016.
- Ayers, G. P., Gillett, R. W., and Gras, J. L.: On the vapour pressure of sulphuric acid, *Geophys. Res. Lett.* 7, 433–436, 1980
- Belyaev, D., Montmessin, F., Bertaux, J. L., Mahieux, A., Fedorova, A., Korablev, O., Marcq, E., Yung, Y.L., Zhang, X.: Vertical profiling of SO₂ and SO above Venus' clouds by SPICAV/SOIR Solar Occultations, *Icarus* 217, 740–751, 2012.
- Berndt, T., Böge, O., Stratmann, F., Heintzenberg, J., and Kulamala, M.: Rapid formation of sulfuric acid particles at near-atmospheric conditions, *Science*, 307, 698–700, 2005.
- Bianchi, F., Dommen, J., Mathot, S., and Baltensperger, U.: On-line determination of ammonia at low pptv mixing ratios in the CLOUD chamber, *Atmos. Meas. Tech.*, 5, 1719–1725, 2012.
- Bianco, R. and Hynes, J. T.: Theoretical studies of heterogeneous reaction mechanisms relevant for stratospheric ozone depletion, *Int. J. Quantum Chem.*, 75, 683–692, 1999.
- Bollas, G. M., Chen, C.–C., and Barton, P. I.: Refined electrolyte–NRTL model: activity coefficient expressions for application to multi–electrolyte systems. *AIChE J.*, 54, 1608–1624, 2008.
- Canagaratna, M. R., Jayne, J. T., Jimenez, J. L., Allan, J. D., Alfarra, M. R., Zhang, Q., Onasch, T. B., Drewnick, F., Coe, H., Middlebrook, A., Delia, A., Williams, L. R., Trimborn, A. M., Northway, M. J., DeCarlo, P. F., Kolb, C. E., Davidovits, P., and Worsnop, D. R.: Chemical and microphysical characterization of ambient aerosols with the Aerodyne aerosol mass spectrometer, *Mass Spectrom. Rev.*, 26, 185–222, 2007.
- Capaldo, K., Corbett, J. J., Kasibhatla, P., Fischbeck, P. and Pandis, S. N.: Effects of ship emissions on sulphur cycling and radiative climate forcing over the ocean, *Nature*, 400, 743–746, 1999.
- Charlson, R. J., Lovelock, J. E., Andreae, M. O., and Warren, S. G.: Oceanic phytoplankton, atmospheric sulphur, cloud albedo and climate, *Nature*, 326, 655–661, 1987.
- Chen, C. C., Britt, H. I., Boston, J. F., Evans, L. B.: Local composition model for excess Gibbs energy of electrolyte systems. Part I: Single solvent, single completely dissociated electrolyte systems. *AIChE J.* 28, 588–596, 1982.
- Clarke, A. D., Davis, D., Kapustin, V. N., Eisele, F., Chen, G., Paluch, I., Lenschow, D., Bandy, A. R., Thornton, D., Moore, K., Mauldin, L., Tanner, D., Litchy, M., Carroll, M. A., Collins, J., Albercook, G.: Particle nucleation in the Tropical boundary layer and its coupling to marine sulfur sources, *Science*, 282, 89–92, 1998a.
- Clegg, S. L., and Brimblecombe, P.: Application of a Multicomponent Thermodynamic Model to Activities and Thermal Properties of 0–40 mol kg⁻¹ Aqueous Sulfuric Acid from <200 to 328 K. *J. Chem. Eng. Data*, 40, 43–64, 1995.



- Clegg, S. L., Brimblecombe, P., and Wexler, A.S.: Thermodynamic model of the system $\text{H}^+ - \text{NH}_4^+ - \text{Na}^+ - \text{SO}_4^{2-} - \text{NO}_3^- - \text{Cl}^- - \text{H}_2\text{O}$ at 298.5 K, *J. Phys. Chem. A*, 102, 2155–2171, 1998.
- Curtius, J., Sierau, B., Arnold, F., Baumann, R., Schulte, P., and Schumann, U.: First direct sulfuric acid detection in the exhaust plume of a jet aircraft in flight, *Geophys. Res. Lett.*, **25**, 923–926, 1998.
- 5 Deshler, T.: A review of global stratospheric aerosol: Measurements, importance, life cycle, and local stratospheric aerosol, *Atmos. Res.*, 90, 223–232, 2008.
- Donahue, T. M., Hoffman, J. H., Hodges, R. R., and Watson, A. J.: Venus was wet: A Measurement of the Ratio of Deuterium to Hydrogen, *Science*, 216, 630–633, 1982.
- Doyle, G. J.: Self-nucleation in the sulphuric acid–water system, *J. Chem. Phys.* 35, 795–799, 1961.
- 10 Drewnick, F., Schneider, J., Hings, S.S., Hock, N., Noone, K., Targino, A., Weimer, S., Borrmann, S.: Measurement of Ambient, Interstitial, and Residual Aerosol Particles on a Mountaintop Site in Central Sweden using an Aerosol Mass Spectrometer and a CVI, *J. Atmos. Chem.* 2006
- Duplissy, J., Merikanto, J., Franchin, A., Tsagkogeorgas, G., Kangasluoma, J., Wimmer, D., Vuollekoski, H., Schobesberger, S., Ehrhart, S., Lehtipalo, K., Flagan, R., Brus, D., Donahue, N., Vehkamäki, H., Almeida, J., Amorim, A., Barmet, P., Bianchi, F., Breitenlechner, M., Dunne, E., Henschel, H., Junninen, H., Kirkby, J., Kurten, A., Kupc, A., Maattanen, A., Makhmutov, V., Napari, I., Nieminen, T., Praplan, A., Riccobono, F., Rondo, L., Steiner, G., Tome, A., Baltensperger, U., Carslaw, K., Dommen, L., Hansel, A., Petaja, T., Sipila, M., Stratmann, F., Vrtala, A., Wagner, P., Worsnop, D., Curtius, J., and Kulmala, M.: Effect of ions on sulfuric acid–water binary particle formation 2: Experimental data and comparison with QC-normalized classical nucleation theory, *J. Geophys. Res. Atmos.*, 121, 1752–1775, 2016, doi:[10.1002/2015JD023539](https://doi.org/10.1002/2015JD023539).
- 15 F., Breitenlechner, M., Dunne, E., Henschel, H., Junninen, H., Kirkby, J., Kurten, A., Kupc, A., Maattanen, A., Makhmutov, V., Napari, I., Nieminen, T., Praplan, A., Riccobono, F., Rondo, L., Steiner, G., Tome, A., Baltensperger, U., Carslaw, K., Dommen, L., Hansel, A., Petaja, T., Sipila, M., Stratmann, F., Vrtala, A., Wagner, P., Worsnop, D., Curtius, J., and Kulmala, M.: Effect of ions on sulfuric acid–water binary particle formation 2: Experimental data and comparison with QC-normalized classical nucleation theory, *J. Geophys. Res. Atmos.*, 121, 1752–1775, 2016, doi:[10.1002/2015JD023539](https://doi.org/10.1002/2015JD023539).
- 20 Eisele, F. L., and Tanner D. J.: Measurement of the gas phase concentrations of H_2SO_4 and methane sulfonic acid and estimates of H_2SO_4 production and loss in the atmosphere, *J. Geophys. Res.*, 98, 9001–9010, 1993.
- Esposito, L. W., Knollenberg, R. G., Marov, M. Y., Toon, O. B. and Turco, R. P.: in: Hunten, D. M., Colin, L., Donahue, T. M. and Moroz, V. I.(Eds.), *Venus*, University Arizona Press, 484–564, 1983.
- Fahey, D. W., Keim, E.R., Boering, K.A., Brock, C.A., Wilson, J.C., Jonsson, H.H., Anthony, S., Hanisco, T.F., Wennberg, P.O., Miake-Lye, R.C., Salawitch, R.J., Louisnard, N., Woodbridge, E.L., Gao, R.S., Donnelly, S.G., Wamsley, R.C., Del Negro, L.A., Solomon, S., Daube, B.C., Wofsy, S.C., Webster, C.R., May, R.D., Kelly, K.K., Loewenstein, M., Podolske, J.R., and Chan. K.R.: Emission measurements of the Concorde supersonic aircraft in the lower stratosphere, *Science*, 270, 70–74, 1995.
- Fan, S.-M. and Jacobs, D. J.: Surface ozone depletion in Arctic spring sustained by bromine reactions on aerosols, *Nature*, 359, 522–524, 1992.
- 30 Fiedler, V., Dal Maso, M., Boy, M., Aufmhoff, H., Hoffmann, J., Schuck, T., Birmili, W., Hanke, M., Uecker, J., Arnold, F., and Kulmala, M.: The contribution of sulphuric acid to atmospheric particle formation and growth: a comparison between boundary layers in Northern and Central Europe, *Atmos. Chem. Phys.*, 5, 1773–1785, 2005.



- Finlayson–Pitts, B. J. and Pitts J. N.: Chemistry of the upper and lower atmosphere: theory, experiments and applications, Academic Press, San Diego, CA, USA, 969 pp., 1999.
- Fuchs, N. A. and Sutugin, A. G.: In Topics in Current Aerosol Research, Pergamon Press, 1971.
- Galloway, J. N. and Rodhe, H.: Regional atmospheric budgets of S and N fluxes: how well can they be quantified? Proc. Roy. Soc. Edinburgh 97B, 61–80, 1991.
- 5 Giauque, W. F., Hornung, E. W., Kunzler, J. E., and Rubin, T. R.: The thermodynamic properties of aqueous sulphuric acid solutions from 15 to 300K, J. Am. Chem. Soc., 82, 62–70, 1960.
- Gmitro, J. T. and Vermeulen, T.: Vapor–liquid equilibria for aqueous sulfuric acid, AIChEJ., 10, 740–746, 1964
- Grädel, T. E. and Crutzen, P. J.: Chemie der Atmosphäre, Bedeutung für Klima und Umwelt (Spektrum, Heidelberg), 1994.
- 10 Hämeri, K., Väkevä, M., Hanson, H.–C., and Laaksonen, A.: Hygroscopic growth of ultrafine ammonium sulphate aerosol measured using an ultrafine tandem differential mobility analyzer, J. Geophys. Res., 105, 22 231–22 242, 2000.
- Hanson, D. R. and Eisele, F.: Diffusion of H₂SO₄ in humidified nitrogen: Hydrated H₂SO₄, J. Phys. Chem., A, 104, 1715–1719, 2000.
- Hanson, D. R. and Ravishankara, A. R.: Heterogeneous Chemistry of Bromine Species in Sulfuric Acid Under Stratospheric
- 15 Conditions, Geophys. Res. Lett., 22, 385–388, 1995.
- Hashimoto, G. L. and Abe, Y.: Stabilization of Venus' climate by a chemical–albedo feedback, Earth Planet, Space, 52, 197–202, 2000.
- Hofmann, D. J.: Aircraft sulfur emissions, Nature, 349, 659, 1991.
- Hofmann, D. J. and Rosen, J. M.: Balloon observations of a particle layer injected by stratospheric aircraft at 23 km, Geophys.
- 20 Res. Lett., 5, 511–514, 1978.
- Hoffman, J. H., Hodges, R. R., Donahue, T. M., and McElroy, M. B.: Composition of the Venus lower atmosphere from the Pioneer Venus mass spectrometer, J. Geophys. Res., 85, 7882–7890, 1980a.
- Hommel, R., Timmreck, C. and Graf, H. F.: The global middle–atmosphere aerosol model MAECHAM5–SAM2: comparison with satellite and in–situ observations, Geosci. Model Dev., 4, 809–834, 2011.
- 25 Huebert, B. J.: Sulphur emissions from ships, Nature, 400, 713–714, 1999.
- Hyvärinen, A.–P., Raatikainen, T., Laaksonen, A., Viisanen, Y., and Lihavainen, H.: Surface tensions and densities of H₂SO₄ + NH₃ + water solutions, Geophys. Res. Lett., 32, L16806, 2005.
- IPCC, 2013: Climate Change 2013: The Physical Science Basis. Contribution of Working Group I to the Fifth Assessment Report of the Intergovernmental Panel on Climate Change [Stocker, T.F., D. Qin, G.–K. Plattner, M. Tignor, S.K. Allen, J.
- 30 Boschung, A. Nauels, Y. Xia, V. Bex and P.M. Midgley (eds.)], Cambridge University Press, Cambridge, United Kingdom and New York, NY, USA, 1535 pp, 2013.
- Jacobson, M. Z.: Fundamentals of Atmospheric Modelling (2nd edition), Cambridge University Press, Cambridge, United Kingdom and New York, NY, USA, ISBN: 0 521 54865 9, 2005a.



- Jayne, J. T., Pöschl, U., Chen, Y., Dai, D., Molina, L. T., Worsnop, D. R., Kolb, C. E., and Molina, M. J.: Pressure and Temperature Dependence of the Gas–Phase Reaction of SO₃ with H₂O and the Heterogeneous Reaction of SO₃ with H₂O / H₂SO₄ Surfaces, *J. Phys. Chem. A*, 101, 10000–10011, 1997.
- Jenkin, M. E., Saunders, S. M., and Pilling, M. J.: The tropospheric degradation of volatile organic compounds: A protocol for
5 mechanism development, *Atmos. Environ.*, 31, 81–104, 1997.
- Jenkin, M. E., Saunders, S. M., Wagner, V., and Pilling, M. J.: Protocol for the development of the Master Chemical Mechanism, MCM v3 (Part B): tropospheric degradation of aromatic volatile organic compounds, *Atmos. Chem. Phys.*, 3, 181–193, 2003.
- Jimenez, J.L., Jayne, J.T., Shi, Q., Kolb, C.E., Worsnop, D.R., Yourshaw, I., Seinfeld, J.H., Flagan, R.C., Zhang, X., Smith,
10 K.A., Morris, J., Davidovits, P.: Ambient aerosol sampling with an aerosol mass spectrometer. *J. Geophys. Res. – Atmospheres* 108 (D7), 8425, 2003a.
- Jimenez, J. L., Canagaratna, M. R., Donahue, N. M., Prevot, A. S. H., Zhang, Q., Kroll, J. H., DeCarlo, P. F., Allan, J. D., Coe, H., Ng, N. L., Aiken, A. C., Docherty, K. S., Ulbrich, I. M., Grieshop, A. P., Robinson, A. L., Duplissy, J., Smith, J. D., Wilson, K. R., Lanz, V. A., Hueglin, C., Sun, Y. L., Tian, J., Laaksonen, A., Raatikainen, T., Rautiainen, J., Vaattovaara, P., Ehn, M.,
15 Kulmala, M., Tomlinson, J. M., Collins, D. R., Cubison, M. J., Dunlea, E. J., Huffman, J. A., Onasch, T. B., Alfarra, M. R., Williams, P. I., Bower, K., Kondo, Y., Schneider, J., Drewnick, F., Borrmann, S., Weimer, S., Demerjian, K., Salcedo, D., Cottrell, L., Griffin, R., Takami, A., Miyoshi, T., Hatakeyama, S., Shimono, A., Sun, J. Y., Zhang, Y. M., Dzepina, K., Kimmel, J. R., Sueper, D., Jayne, J. T., Herndon, S. C., Trimborn, A. M., Williams, L. R., Wood, E. C., Middlebrook, A. M., Kolb, C. E., Baltensperger, U., and Worsnop, D. R.: Evolution of Organic Aerosols in the Atmosphere, *Science*, 326, 1525–1529, 2009.
- 20 Junge, C.: The chemical composition of atmospheric aerosols, I, Measurements at Round Hill field station, June–July 1953, *J. Meteorol.*, 11, 323, 1954.
- Junge, C. E.: Sulfur in the atmosphere, *J. Geophys. Res.*, 68(13), 3975–3976, 1963.
- Junge, E., Chagnon, C. W. and Manson J. E.: A world–wide stratospheric aerosol layer, *Science*, 133, 1478–1479, 1961.
- Kiang, C. S., Stauffer, D.: Chemical nucleation theory for various humidities and pollutants, *Faraday Symp. Chem. Soc.*, 7,
25 26–33, 1973.
- Kiene, R. P.: Sulphur in the mix, *Nature*, 402, 363–365, 1999.
- King, H. H., Hall, J. L., and Ware, G. C.: A study of the density, surface tension and adsorption in the water–ammonia system at 20°, *J. Am. Chem. Soc.*, 52, 5128–5135, 1930.
- Kirkby, J., Curtius, J., Almeida, J., Dunne, E., Duplissy, J., Ehrhart, S., Franchin, A., Gagné, S., Ickes, L., Kürten, A., Kupc,
30 A., Metzger, A., Riccobono, F., Rondo, L., Schobesberger, S., Tsagkogeorgas, G., Wimmer, D., Amorim, A., Bianchi, F., Breitenlechner, M., David, A., Dommen, J., Downard, A., Ehn, M., Flagan, R., Haider, S., Hansel, A., Hauser, D., Jud, W., Junninen, H., Kreissl, F., Kvashin, A., Laaksonen, A., Lehtipalo, K., Lima, J., Lovejoy, E., Makhmutov, V., Mathot, S., Mikkilä, J., Minginette, P., Mogo, S., Nieminen, T., Onnela, A., Pereira, P., Petäjä, T., Schnitzhofer, R., Seinfeld, J., Sipilä, M., Stozhkov, Y., Stratmann, F., Tomé, A., Vanhanen, J., Viisanen, Y., Aron Vrtala, A., Wagner, P., Walther, H., Weingartner,



- E., Wex, H., Winkler, P., Carslaw, K., Worsnop, D., Baltensperger, U. and Kulmala, M.: Role of sulphuric acid, ammonia and galactic cosmic rays in atmospheric aerosol nucleation, *Nature*, 476, 429–433, 2011.
- Koehler, H. W.: Results of the Venus sondes Venera 13 and 14, *Sterne und Weltraum* 21: 282, 1982.
- Koop, T. and Carslaw, K.S.: Melting of $\text{H}_2\text{SO}_4 \cdot 4\text{H}_2\text{O}$ particles upon cooling: Implications for polar stratospheric clouds, *Science*, 272, 1638–1641, 1996.
- Kokkola, H., Hommel, R., Kazil, J., Niemeier, U., Partanen, A.–I., Feichter, J., and Timmreck, C.: Aerosol microphysics modules in the framework of the ECHAM5 climate model –intercomparison under stratospheric conditions, *Geosci. Model Dev.*, 2, 97–112, 2009.
- Korhonen, P., Laaksonen, A., Batris, E., and Viisanen, Y.: Thermodynamics for highly concentrated water–ammonium sulfate solutions, *J. Aerosol Sci.*, 29, 379–380, 1998b.
- Krasnopolsky, V. A. and Parshev, V. A.: Chemical composition of the atmosphere of Venus, *Nature* 292 (5824): 610–613, 1981.
- Krasnopolsky, V. A.: Chemical composition of Venus atmosphere and clouds: Some unsolved problems, *Planetary and Space Science* 54 (13–14): 1352–1359, 2006b.
- Kuang, C., McMurry, P. H., McCormick, A. V., and Eisele, F. L.: Dependence of nucleation rates on sulfuric acid vapor concentration in diverse atmospheric locations, *J. Geophys. Res.*, 113, D10209, 2008.
- Kulmala, M. and Laaksonen, A.: Binary nucleation of water–sulfuric acid system: Comparison of classical theories with different H_2SO_4 saturation vapor pressures, *J. Chem. Phys.*, 93, 696–701, 1990.
- Kulmala, M., Pirjola, L., and Mäkelä, J. M.: Stable sulphate clusters as a source of new atmospheric particles, *Nature* 404, 66–69, 2000.
- Kulmala, M., Vehkamäki, H., Petäjä, T., Maso, M. D., Lauri, A., Kerminen, V.–M., Birmili, W., and McMurry, P.: Formation and growth rates of ultrafine atmospheric particles: a review of observations, *J. Aerosol Sci.*, 35, 143–176, 2004.
- Kupc, A., Amorim, A., Curtius, J., Danielczok, A., Duplissy, J., Ehrhart, S., Walther, H., Ickes, L., Kirkby, J., Kurten, A., Lima, J. M., Mathot, S., Minginette, P., Onnela, A., Rondo, L., and Wagner, P. E.: A fibre–optic UV system for H_2SO_4 production in aerosol chambers causing minimal thermal effects, *Journal of Aerosol Science*, 42, 532–543, 2011.
- Kürten, A., Rondo, L., Ehrhart, S., and Curtius, J.: Performance of a corona ion source for measurement of sulfuric acid by chemical ionization mass spectrometry, *Atmos. Meas. Technol.*, 4, 437–443, doi: 10.5194/amt-4-437-2011, 2011.
- Kürten, A., Rondo, L., Ehrhart, S. and Curtius, J.: Calibration of a Chemical Ionization Mass Spectrometer for the Measurement of Gaseous Sulfuric Acid, *J. Phys. Chem. A*, 116(24), 6375–6386, doi: 10.1021/jp212123n, 2012.
- Laaksonen, A. and Kulmala, M.: Homogeneous heteromolecular nucleation of sulphuric acid and water vapours in stratospheric conditions: A theoretical study of the effect of hydrate interaction, *J. Aerosol Sci.*, 22, 779–787, 1991.
- Lai, A. and Nazaroff, W. W.: Modelling indoor particle deposition from turbulent flow onto smooth surfaces, *J. Aerosol Sci.*, 31, 463–476, 2000.



- Lehtinen, K. E. J. and Kulmala, M.: A model for particle formation and growth in the atmosphere with molecular resolution in size, *Atmos. Chem. Phys.*, 3, 251–257, 2003.
- Lörting, T. and Liedl, K. R.: Toward elimination of discrepancies between theory and experiment: The rate constant of the atmospheric conversion of SO_3 to H_2SO_4 , *PNAS*, 97, 16, 8874–8878, 2000.
- 5 Margarella, A. M., Perrine, K. A., Lewis, T., Faubel, M., Winter, B., and Hemminger, J. C.: Dissociation of sulfuric acid in aqueous solution: Determination of the photoelectron spectral fingerprints of H_2SO_4 , HSO_4^- , and SO_4^{2-} in water, *J. Phys. Chem. C*, 117, 8131–8137, 2013.
- Marti, J. J., Jefferson, A., Ping Cai, X., Richert, C., McMurry, P. H., Eisele, F.: H_2SO_4 vapor pressure of sulfuric acid and ammonium sulfate solutions, *J. Geophys. Res.*, 102, D3, 3725–3735, 1997.
- 10 Mauldin, R. L., III, Cantrell, C. A., Zondlo, M., Kosciuch, E., Eisele, F. L., Chen, G., Davis, D., Weber, R., Crawford, J., Blake, D., Bandy, A., and Thornton, D.: Highlights of OH, H_2SO_4 , and methane sulfonic acid measurements made aboard the NASA P-3B during Transport and Chemical Evolution over the Pacific, *J. Geophys. Res.*, 108(D20), 8796, 2003.
- McNamara, J. P. and Hillier, I. H.: Structure and reactivity of dinitrogen pentoxide in small water clusters studied by electronic structure calculations, *J. Phys. Chem. A*, 104, 5307–5319, 2000.
- 15 Merikanto, J., Spracklen, D. V., Mann, G. W., Pickering, S. J., and Carslaw, K. S.: Impact of nucleation on global CCN, *Atmos. Chem. Phys.*, 9, 8601–8616, 2009.
- Miake-Lye, R. C., Anderson, B. E., Cofer, W. R., Wallio, H. A., Nowicki, G. D., Ballenthin, J. O., Hunton, D. E., Knighton, W. B., Miller, T. M., Seeley, J. V., and Viggiano, A. A.: SO_x Oxidation and Volatile Aerosol in Aircraft Exhaust Plumes Depend on Fuel Sulfur Content, *Geophys. Res. Lett.*, 25, 10, 1677–1680, 1998.
- 20 Mills, F. P., Esposito, L. W., and Yung, Y. L.: Atmospheric composition, chemistry, and clouds, In: Esposito, L. W., Stofan, E. R. and Cravens, T. E. (Eds.), *Exploring Venus as a Terrestrial Planet*, American Geophysical Union, Washington, DC, 73–100, 2007.
- Molina, M. J., Zhang, R., Wooldridge, P. J., McMahan, J. R., Kim, J. E., Chang, H. Y., and Beyer, K. D.: Physical Chemistry of the $\text{H}_2\text{SO}_4/\text{HNO}_3/\text{H}_2\text{O}$ System: Implications for the Formation of Polar Stratospheric Clouds, *Science*, 261, 1418–1423, 25 1993.
- Morokuma, K. and Muguruma, C.: Ab-initio molecular-orbital study of the mechanism of the gas-phase reaction $\text{SO}_3 + \text{H}_2\text{O}$ – Importance of the 2nd water molecule, *J. Am. Chem. Soc.* 116, 10316–10317, 1994.
- Moroz, V. I., Parfent'ev, N.A., and San'ko, N.F.: Spectrophotometric experiment on the Venera 11 and 12 descent modules. 2. Analysis of Venera 11 spectra by layer-addition method, *Cosmis. Res.* 17, 601–614, 1979.
- 30 Nickless, G.: Ed. "Inorganic Sulfur Chemistry", Elsevier, Amsterdam, 1968.
- Noppel, M., H. Vehkamäki, and M. Kulmala, An improved model for hydrate formation in sulfuric-acid water nucleation, *J. Chem. Phys.* 116, 218–228, 2002.
- Öm, G., Hansson U., and Rodhe, H.: Historical worldwide emissions of anthropogenic sulfur: 1860–1985, Department of Meteorology, Stockholm University, Report CM-91, 1996.



- Petters, M. D. and Kreidenweis, S. M.: A single parameter representation of hygroscopic growth and cloud condensation nucleus activity, *Atmos. Chem. Phys.*, 7, 1961–1971, 2007.
- Pierce, J. R. and Adams, P. J.: Uncertainty in global CCN concentrations from uncertain aerosol nucleation and primary emission rates, *Atmos. Chem. Phys.*, 9, 1339–1356, 2009.
- 5 Pöschl, U., Canagaratna, M., Jayne, J. T., Molina, L. T., Worsnop, D. R., Kolb, C. E., and Molina, M. J.: Mass accommodation coefficient of H₂SO₄ vapor on aqueous sulfuric acid surfaces and gaseous diffusion coefficient of H₂SO₄ in N₂/H₂O, *J. Phys. Chem. A* 102:10082–10089, 1998.
- Prinn, R. G.: Venus: Composition and Structure of the Visible Clouds, *Science*, 182, 1132–1135, 1973.
- Que, H., Song, Y., and Chen, C.: Thermodynamic modeling of the sulfuric acid–water–sulfur trioxide system with the symmetric Electrolyte NRTL model. *J. Chem. Eng. Data*, 56, 963–977, 2011.
- 10 Richardson, C. B., R. L. Hightower, and A. L. Pigg, Optical measurement of the evaporation of sulfuric acid droplets, *Appl. Opt.*, 25, 1226–1229, 1986.
- Rodhe, H.: Human impact on the atmospheric sulfur balance. *Tellus*, 51A–B, 110–122, 1999.
- Robinson, G. N., Worsnop, D. R., Jayne, J. T., Kolb, C. E., and Davidovits, P.: Heterogeneous Uptake of ClONO₂ and N₂O₅ by Sulfuric Acid Solutions, *J. Geophys. Res.*, 102, 3583–3601, 1997.
- 15 Roedel, W.: Measurements of sulfuric acid saturation vapor pressure: Implications for aerosol formation by heteromolecular nucleation, *J. Aerosol Sci.*, 10, 375–386, 1979.
- Roldin, P., Eriksson, A. C., Nordin, E. Z., Hermansson, E., Mogensen, D., Rusanen, A., Boy, M., Swietlicki, E., Svenningsson, B., Zelenyuk, A., and Pagels, J: Modelling non–equilibrium secondary organic aerosol formation and evaporation with the aerosol dynamics, gas– and particle–phase chemistry kinetic multilayer model ADCHAM, *Atmos. Chem. Phys.*, 14, 7953–7993, 2014.
- 20 Roldin, P., Liao, L., Mogensen, D., Dal Maso, M., Rusanen, A., Kerminen, V.–M., Mentel, T. F., Wildt, J., Kleist, E., Kiendler–Scharr, A., Tillmann, R., Ehn, M., Kulmala, M., and Boy, M.: Modelling the contribution of biogenic volatile organic compounds to new particle formation in the Jülich plant atmosphere chamber, *Atmos. Chem. Phys.*, 15, 10777–10798, 25 2015.
- Saunders, S. M., Jenkin, M. E., Derwent, R. G., and Pilling, M. J.: Protocol for the development of the Master Chemical Mechanism, MCM v3 (Part A): tropospheric degradation of nonaromatic volatile organic compounds, *Atmos. Chem. Phys.*, 3, 161–180, 2003.
- Schnitzhofer, R., Metzger, A., Breitenlechner, M., Jud, W., Heinritzi, M., De Menezes, L.–P., Duplissy, J., Guida, R., Haider, S., Kirkby, J., Mathot, S., Minginette, P., Onnela, A., Walther, H., Wasem, A., Hansel, A., and the CLOUD Team: Characterisation of organic contaminants in the CLOUD chamber at CERN, *Atmos. Meas. Tech.*, 7, 2159–2168, 2014.
- 30 Schreiner, J., Voigt, C., Kohlmann, A., Arnold, F., Mauersberger, K., and Larsen, N.: Chemical analysis of polar stratospheric cloud particles, *Science* 283, 968–970, 1999.



- Schumann, U., Strom, J., Busen, R., Baumann, R., Gierens, K., Krautstrunk, M., Schröder, F. P., and Stingl, J.: In situ observations of particles in jet aircraft exhausts and contrails for different sulfur-containing fuels, *J. Geophys. Res.*, 101, 6853–6869, 1996.
- Simó, R. and Pedrós–Alió, C.: Role of vertical mixing in controlling the oceanic production of dimethyl sulphide, *Nature*, 402, 396–399, 1999.
- Simpson, D., Fagerli, H., Hellsten, S., Knulst, J. C., and Westling O.: Comparison of modelled and monitored deposition fluxes of sulphur and nitrogen to ICP-forest sites in Europe, *Biogeosciences*, 3, 337–355, 2006.
- Smith, S. J., Pitcher, H., and Wigley, T. M. L: Global and Regional Anthropogenic Sulfur Dioxide Emissions, *Global Planet. Change*, 29(1–2), 99–119, 2001.
- Solomon, S., Garcia, R. R., Rowland, F. S., Wuebbles, D. J.: On the depletion of Antarctic ozone, *Nature*, 321, 755–758, 1986.
- Solomon, S.: Stratospheric ozone depletion: A review of concepts and history, *Rev. Geophys.*, 37, 3, 275–316, 1999.
- Solomon, S. C., Bullock, M. A., and Grinspoon, D. H.: Climate Change as a Regulator of Tectonics on Venus, *Science*, 286, 87–90, 1999.
- Solomon, S., Daniel, J. S., Neely III, R. R., Vernier, J.–P., Dutton, E. G., and Thomason, L. W.: The Persistently Variable “Background” Stratospheric Aerosol Layer and Global Climate Change, *Science*, 333, 866, 2011.
- Song, Y. and Chen, C.–C.: Symmetric Electrolyte Nonrandom Two–Liquid Activity Coefficient Model. *Ind. Eng. Chem. Res.*, 48, 7788–7797, 2009.
- Stauffer, D.: Kinetic theory of two–component (“heteromolecular”) nucleation and condensation, *J. Aerosol Sci.*, 7, 319–333, 1976.
- Studel, R.: Sulfuric acid from sulfur trioxide and water – A Surprisingly complex reaction, *Angew. Chem. Int. Ed.* 34, 1313–1315, 1995.
- Stockwell, W. R. and Calvert, J. G.: The mechanism of the HO–SO₂ reaction, *Atmos. Environ.* 17, 2231–2235, 1983b.
- Sullivan, R. C., Petters, M. D., DeMott, P. J., Kreidenweis, S. M., Wex, H., Niedermeier, D., Hartmann, S., Clauss, T., Stratmann, F., Reitz, P., Schneider, J., and Sierau, B.: Irreversible loss of ice nucleation active sites in mineral dust particles caused by sulphuric acid condensation, *Atmos. Chem. Phys.*, 10, 11471–11487, 2010.
- Tang, I. N., and Munkelwitz, H. R.: An investigation of solute nucleation in levitated solution droplets, *J. Colloid. Interface Sci.*, 98, 430–438, 1984.
- Toon, O. B. and Tolbert, M. A.: Spectroscopic evidence against nitric acid trihydrate in polar stratospheric clouds, *Nature*, 375, 218–221, 1995.
- Turco, R.P., Whitten, R.C., and Toon, O.B.: Stratospheric aerosols: Observation and theory, *Rev. Geophys. Space Phys.*, 20, 233–279, 1982.
- Vaida, V., Kjaergaard, H. G., Hintze, P. E., and Donaldson, D. J.: Photolysis of sulfuric acid vapor by visible solar radiation, *Science*, 299, 1566–1568, 2003.



- Vehkamäki, H., Kulmala, M., Napari, I., Lehtinen, K. E. J., Timmreck, C., Noppel, M., and Laaksonen, A.: An improved parameterization for sulfuric acid–water nucleation rates for tropospheric and stratospheric conditions, *J. Geophys. Res.*, 107(D22), 4622, 2002.
- Voigtländer, J., Duplissy, J., Rondo, L., Kürten, A., and Stratmann, F.: Numerical simulations of mixing conditions and aerosol dynamics in the CERN CLOUD chamber, *Atmos. Chem. Phys.*, 12, 2205–2214, 2012.
- Volmer, M. and Weber, A.: Keimbildung in übersättigten Gebilden, *Z. Phys. Chem.*, 119, 277, 1926.
- Walrafen, G. E., Yang, W. H., Chu, Y. C., Hokmabadi, M. S.: Structures of Concentrated Sulfuric Acid Determined from Density, Conductivity, Viscosity, and Raman Spectroscopic Data, *J. Solution Chem.*, 29, 905–936, 2000.
- Wang, P., Anderko, A., Springer, R. D., and Young, R. D.: Modeling Phase Equilibria and Speciation in Mixed–Solvent Electrolyte Systems: II. Liquid–Liquid Equilibria and Properties of Associating Electrolyte Solutions. *J. Mol. Liq.*, 125, 37–44, 2006.
- Wang, S. C. and Flagan, R. C.: Scanning electrical mobility spectrometer, *Aerosol Science and Technology* 13.2, 230–240, 1990.
- Wang, Z. B., Hu, M., Mogensen, D., Yue, D. L., Zheng, J., Zhang, R. Y., Liu, Y., Yuan, B., Li, X., Shao, M., Zhou, L., Wu, Z. J., Wiedensohler, A., and Boy, M.: The simulations of sulfuric acid concentration and new particle formation in an urban atmosphere in China, *Atmos. Chem. Phys.*, 13, 11157–11167, 2013
- Weber, R. J., McMurry, P. H., Mauldin, R. L., Tanner, D. J., Eisele, F. L., Clarke, A. D., and Kapustin, V. N.: New Particle Formation in the Remote Troposphere: A Comparison of Observations at Various Sites, *Geophys. Res. Lett.*, 26, 307–310, 1999.
- Wen, H. and Carignan, J.: Reviews on atmospheric selenium: Emissions, speciation and fate, *Atmos. Env.*, 41, 7151–7165, 2007.
- Wilson, J. C., Jonsson, H. H., Brock, C. A., Toohey, D. W., Avallone, L. M., Baumgardner, D., Dye, J. E., Poole, L. R., Woods, D. C., DeCoursey, R. J., Osborn, M., Pitts, M. C., Kelly, K. K., Chan, K. R., Ferry, G. V., Loewenstein, M., Podolske, J. R., Weaver, A.: In situ observations of aerosol and chlorine monoxide after the 1991 eruption of Mount Pinatubo: effect of reactions on sulfate aerosol, *Science*, 261, 1140–1143, 1993.
- Yu, F. and Luo, G.: Simulation of particle size distribution with a global aerosol model: contribution of nucleation to aerosol and CCN number concentrations, *Atmos. Chem. Phys.*, 9, 7691–7710, 2009.
- Yu, F. and Turco, R. P.: The formation and evolution of aerosols in stratospheric aircraft plumes: Numerical simulations and comparisons with observations, *J. Geophys. Res.*, 103, 915–934, 1998.
- Yu, F. and Turco, R. P.: From molecular clusters to nanoparticles: Role of ambient ionization in tropospheric aerosol formation, *J. Geophys. Res.–Atmos.*, 106, 4797–4814, 2001.
- Zhang, X., Liang, M. C., Montmessin, F., Bertaux, J. L., Parkinson, C., and Yung, Y. L.: Photolysis of sulphuric acid as the source of sulphur oxides in the mesosphere of Venus, *Nature*, 3, 834–837, 2010.



Zhang, X., Liang, M. C., Mills, F., Belyaev, D., and Yung, Y. L.: Sulfur chemistry in the middle atmosphere of Venus, *Icarus*, 217, 714–739, 2012.

Zuend, A., Marcolli, C., Luo, B. P., and Peter, T.: A thermodynamic model of mixed organic–inorganic aerosols to predict activity coefficients, *Atmos. Chem. Phys.*, 8, 4559–4593, 2008.

- 5 Zuend, A., Marcolli, C., Booth, A. M., Lienhard, D. M., Soonsin, V., Krieger, U. K., Topping, D. O., McFiggans G., Peter, T., and Seinfeld, J. H.: New and extended parameterization of the thermodynamic model AIOMFAC: calculation of activity coefficients for organic–inorganic mixtures containing carboxyl, hydroxyl, carbonyl, ether, ester, alkenyl, alkyl, and aromatic functional groups, *Atmos. Chem. Phys.*, 11, 9155–9206, 2011.

10

15

20

25

30



Table 1. The table provides a summary of the experimental conditions (temperature, relative humidity, sulphuric acid gaseous concentration) for each experiment.

Run No	CLOUD Run No	T (K)	RH (%)	[H ₂ SO ₄] _(g) , peak (# cm ⁻³)	[H ₂ SO ₄] _(g) , background (# cm ⁻³)	p _{sat,H2SO4} , peak (Pa)	p _{sat,H2SO4} , background (Pa)
1	914.01	288.8	10.1–0.5	6.0·10 ⁷	1.2·10 ⁷	2.3·10 ⁻⁷	5.0·10 ⁻⁸
2	914.06	288.8	3.5–0.5	2.3·10 ⁸	1.0·10 ⁸	9.0·10 ⁻⁷	4.2·10 ⁻⁷
3	919.02–04	268.0– 293.0	1.4–0.3	1.8·10 ⁹	2.0·10 ⁸	6.3·10 ⁻⁶	2.7·10 ⁻⁷

5

10

15

20



Table 2. Coefficient of determination (R^2) between the modelled and measured GMD for experiments 1, 2 and 3. Also the simulation number that we refer to in the text, the Case with the corresponding values for the equilibrium coefficients $K_{H_2SO_4, 288.8\text{ K}}$ and $K_{SO_3, 288.8\text{ K}}$, the $B_{H_2SO_4}$ and B_{SO_3} values (cf. Eq. 21) to describe the temperature dependence of $K_{H_2SO_4}$ and K_{SO_3} , the assumed species composition of the particle contamination (Con.), and the source to the pure-liquid saturation vapour pressure parameterizations are given.

Exp. No.	Sim. No	Case	$B_{H_2SO_4}$ (K)	B_{SO_3} (K)	$K_{H_2SO_4, 288.8\text{ K}}$ ($\text{mol}\cdot\text{kg}^{-1}$)	$K_{SO_3, 288.8\text{ K}}$	Con.	Vap. pres.	R^2
1	1	^a 1	0	0	$2.00\cdot 10^9$	∞	NH ₃	N–K–L, Nickless	0.994
1	2	^b 2a	0	0	$2.40\cdot 10^9$	$1.43\cdot 10^{10}$	NH ₃	N–K–L, Nickless	0.994
1	3	^c 2b	0	0	$4.00\cdot 10^9$	$1.54\cdot 10^9$	NH ₃	N–K–L, Nickless	0.996
1	4	^d 3	0	0	$1.00\cdot 10^{11}$	$3.33\cdot 10^7$	NH ₃	N–K–L, Nickless	0.992
1	5	1	0	0	**	∞	Org.	N–K–L, Nickless	0.992
1	6	2a	0	0	$2.40\cdot 10^9$	$1.43\cdot 10^{10}$	Org.	N–K–L, Nickless	0.995
1	7	2a	0	0	$2.40\cdot 10^9$	$1.43\cdot 10^{10}$	DMA	N–K–L, Nickless	0.993
1	8	1	0	0	$3.80\cdot 10^9$	∞	NH ₃	ASPEN	0.990
1	9	2a	0	0	$4.00\cdot 10^9$	$4.55\cdot 10^{10}$	NH ₃	ASPEN	0.993
1	10	2b	0	0	$5.00\cdot 10^9$	$5.00\cdot 10^9$	NH ₃	ASPEN	0.995
1	11	3	0	0	$1.00\cdot 10^{11}$	$5.00\cdot 10^7$	NH ₃	ASPEN	0.990
1	12	1	0	0	**	∞	Org.	ASPEN	0.888
2	13	1	0	0	$2.00\cdot 10^9$	∞	NH ₃	N–K–L, Nickless	0.870
2	14	2a	0	0	$2.40\cdot 10^9$	$1.43\cdot 10^{10}$	NH ₃	N–K–L, Nickless	0.869
2	15	2b	0	0	$4.00\cdot 10^9$	$1.54\cdot 10^9$	NH ₃	N–K–L, Nickless	0.871
2	16	3	0	0	$1.00\cdot 10^{11}$	$3.33\cdot 10^7$	NH ₃	N–K–L, Nickless	0.868
2	17	2a	0	0	$2.40\cdot 10^9$	$1.43\cdot 10^{10}$	Org.	N–K–L, Nickless	0.870
2	18	2a	0	0	$2.40\cdot 10^9$	$1.43\cdot 10^{10}$	DMA	N–K–L, Nickless	0.869
2	19	1	0	0	**	∞	Org.	N–K–L, Nickless	0.868
2	20	1	0	0	$3.80\cdot 10^9$	∞	NH ₃	ASPEN	0.867
2	21	2a	0	0	$4.00\cdot 10^9$	$4.55\cdot 10^{10}$	NH ₃	ASPEN	0.870
2	22	2b	0	0	$5.00\cdot 10^9$	$5.00\cdot 10^9$	NH ₃	ASPEN	0.871
2	23	3	0	0	$1.00\cdot 10^{11}$	$5.00\cdot 10^7$	NH ₃	ASPEN	0.867
2	24	1	0	0	**	∞	Org.	ASPEN	0.510
3	25	1	0	0	$2.00\cdot 10^9$	∞	NH ₃	N–K–L, Nickless	0.841
3	26	1	0	0	$2.00\cdot 10^9$	∞	Org.	N–K–L, Nickless	0.905
3	27	1	3475 ^e	0	$2.00\cdot 10^9$	∞	NH ₃	N–K–L, Nickless	0.534



3	28	1	0	0	**	∞	Org.	N-K-L, Nickless	0.967
3	29	2a	3475 [*]	14245.7 [*]	2.40·10 ⁹	1.43·10 ¹⁰	NH ₃	N-K-L, Nickless	0.611
3	30	2a	3475 [*]	0	2.40·10 ⁹	1.43·10 ¹⁰	NH ₃	N-K-L, Nickless	0.825
3	31	2a	3475 [*]	-10000	2.40·10 ⁹	1.43·10 ¹⁰	NH ₃	N-K-L, Nickless	0.992
3	32	2a	0	14245.7 [*]	2.40·10 ⁹	1.43·10 ¹⁰	NH ₃	N-K-L, Nickless	0.839
3	33	2a	0	0	2.40·10 ⁹	1.43·10 ¹⁰	NH ₃	N-K-L, Nickless	0.981
3	34	2a	0	0	2.40·10 ⁹	1.43·10 ¹⁰	Org.	N-K-L, Nickless	0.991
3	35	2a	0	-10000	2.40·10 ⁹	1.43·10 ¹⁰	NH ₃	N-K-L, Nickless	0.860
3	36	2a	0	-3000	2.40·10 ⁹	1.43·10 ¹⁰	NH ₃	N-K-L, Nickless	0.993
3	37	2b	3475 [*]	14245.7 [*]	4.00·10 ⁹	1.54·10 ⁹	NH ₃	N-K-L, Nickless	0.937
3	38	2b	3475 [*]	0	4.00·10 ⁹	1.54·10 ⁹	NH ₃	N-K-L, Nickless	0.819
3	39	2b	3475 [*]	-10000	4.00·10 ⁹	1.54·10 ⁹	NH ₃	N-K-L, Nickless	0.458
3	40	2b	3475 [*]	5000	4.00·10 ⁹	1.54·10 ⁹	NH ₃	N-K-L, Nickless	0.918
3	41	2b	0	14245.7 [*]	4.00·10 ⁹	1.54·10 ⁹	NH ₃	N-K-L, Nickless	0.953
3	42	2b	0	0	4.00·10 ⁹	1.54·10 ⁹	NH ₃	N-K-L, Nickless	0.685
3	43	2b	0	-10000	4.00·10 ⁹	1.54·10 ⁹	NH ₃	N-K-L, Nickless	0.260
3	44	3	3475 [*]	14245.7 [*]	1.00·10 ¹¹	3.33·10 ⁷	NH ₃	N-K-L, Nickless	0.903
3	45	3	3475 [*]	0	1.00·10 ¹¹	3.33·10 ⁷	NH ₃	N-K-L, Nickless	0.571
3	46	3	3475 [*]	-10000	1.00·10 ¹¹	3.33·10 ⁷	NH ₃	N-K-L, Nickless	0.146
3	47	3	0	14245.7 [*]	1.00·10 ¹¹	3.33·10 ⁷	NH ₃	N-K-L, Nickless	0.898
3	48	3	0	0	1.00·10 ¹¹	3.33·10 ⁷	NH ₃	N-K-L, Nickless	0.420
3	49	3	0	-10000	1.00·10 ¹¹	3.33·10 ⁷	NH ₃	N-K-L, Nickless	0.138
3	50	1	0	0	3.80·10 ⁹	∞	NH ₃	ASPEN	0.991
3	51	2a	0	0	4.00·10 ⁹	4.55·10 ¹⁰	NH ₃	ASPEN	0.992
3	52	2b	0	0	5.00·10 ⁹	5.00·10 ⁹	NH ₃	ASPEN	0.880
3	53	3	0	0	1.00·10 ¹¹	5.00·10 ⁷	NH ₃	ASPEN	0.540

* Values from Que et al. (2011).

** Simulation with the H₂SO₄ activity derived from Eq. 14 using the thermodynamic data from Giauque et al. (1960)

^a Case 1: Only evaporation of H₂SO₄.

^b Case 2a: Both H₂SO₄ and SO₃ evaporate from the particles. H₂SO₄ is the main evaporating species at $T=288.8$ K.



^c Case 2b: Both H_2SO_4 and SO_3 evaporate from the particles. SO_3 is the main evaporating species at $T=288.8\text{ K}$.

^d Case 3: SO_3 is completely dominating the evaporation.

5

10

15



ADCHAM model optimized –
 sulfur particle evaporation at low RH

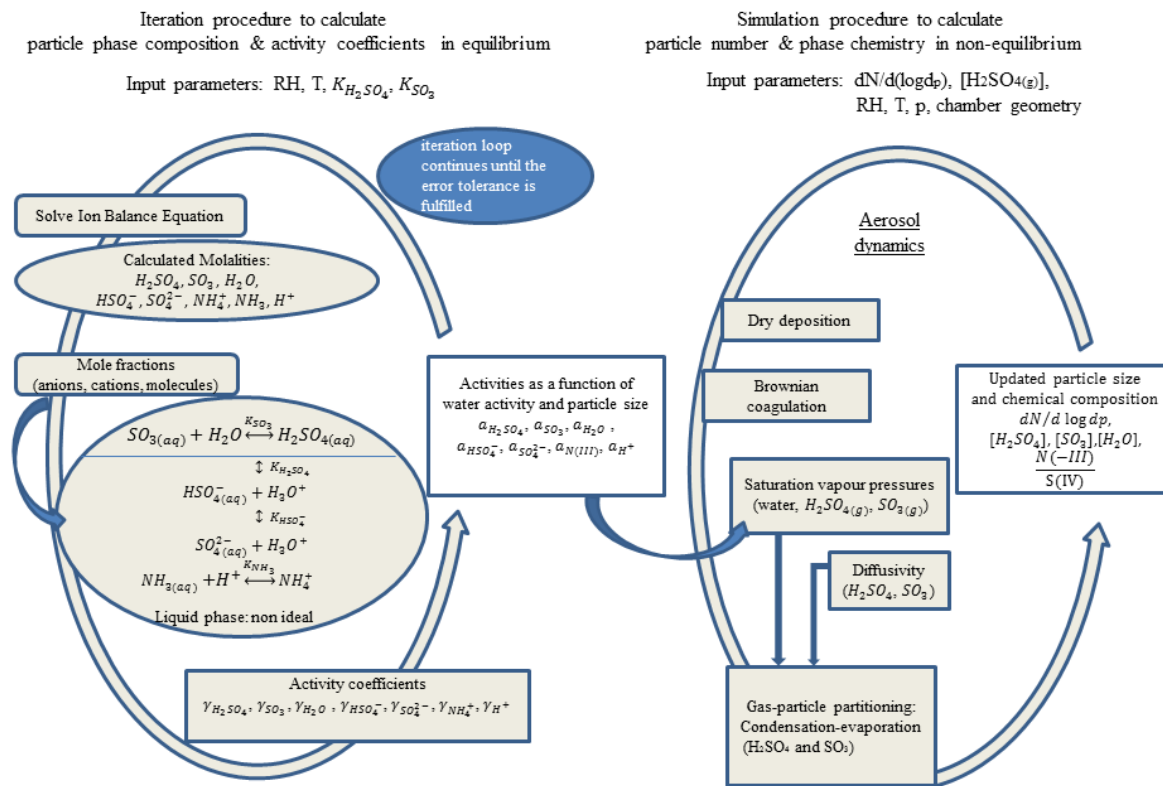
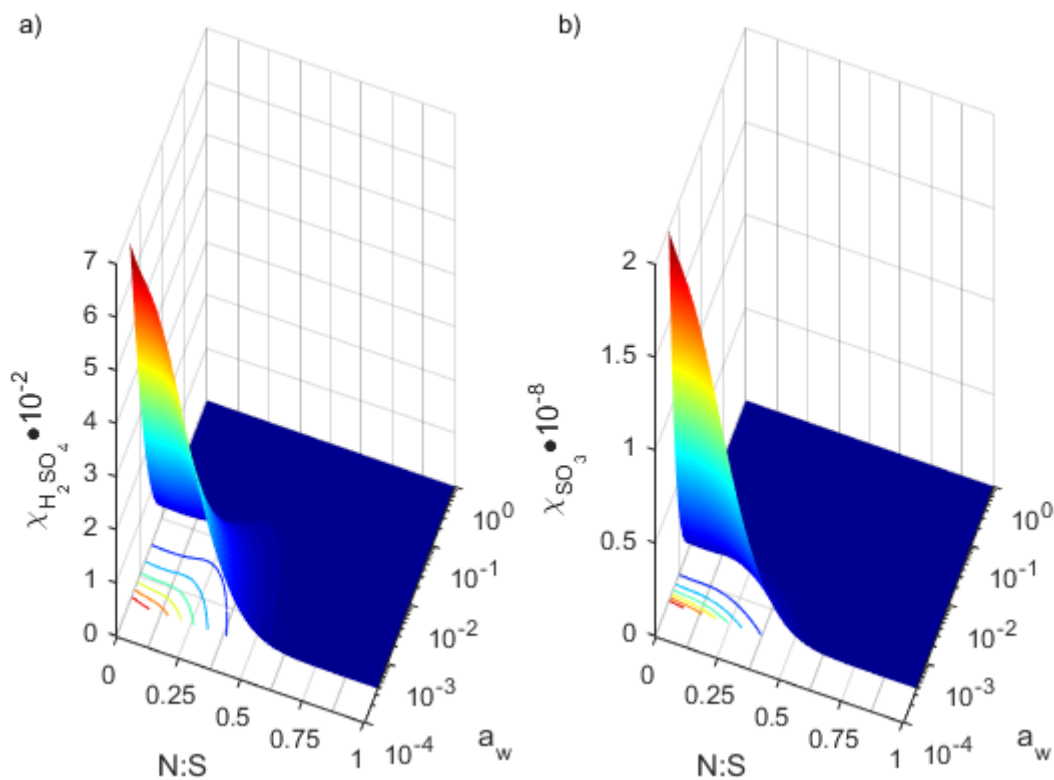


Figure 1. Schematic of the ADCHAM model optimized for the sulphur particle evaporation at low RH.



5 **Figure 2. Modelled particle–phase mole fractions of (a) $\text{H}_2\text{SO}_{4(\text{aq})}$, $\chi_{\text{H}_2\text{SO}_4}$, and (b) $\text{SO}_{3(\text{aq})}$, χ_{SO_3} , as a function of the water activity (a_w) and the N:S for Case 2a which represents the combination of H_2SO_4 , H_2O and SO_3 evaporating species with H_2SO_4 being the dominating evaporating S(VI) species. The colour coded contours on x–y axes represent constant particle–phase mole fractions for a) $\chi_{\text{H}_2\text{SO}_4}=1-6\cdot 10^{-2}$ and b) $\chi_{\text{SO}_3}=0.3-1.8\cdot 10^{-8}$. The equilibrium coefficients for reactions R1 and R3 are $K_{\text{H}_2\text{SO}_4}=2.40\cdot 10^9 \text{ mol}\cdot\text{kg}^{-1}$, and $^*K_{\text{SO}_3}=1.43\cdot 10^{10}$ at $T=288.8 \text{ K}$.**

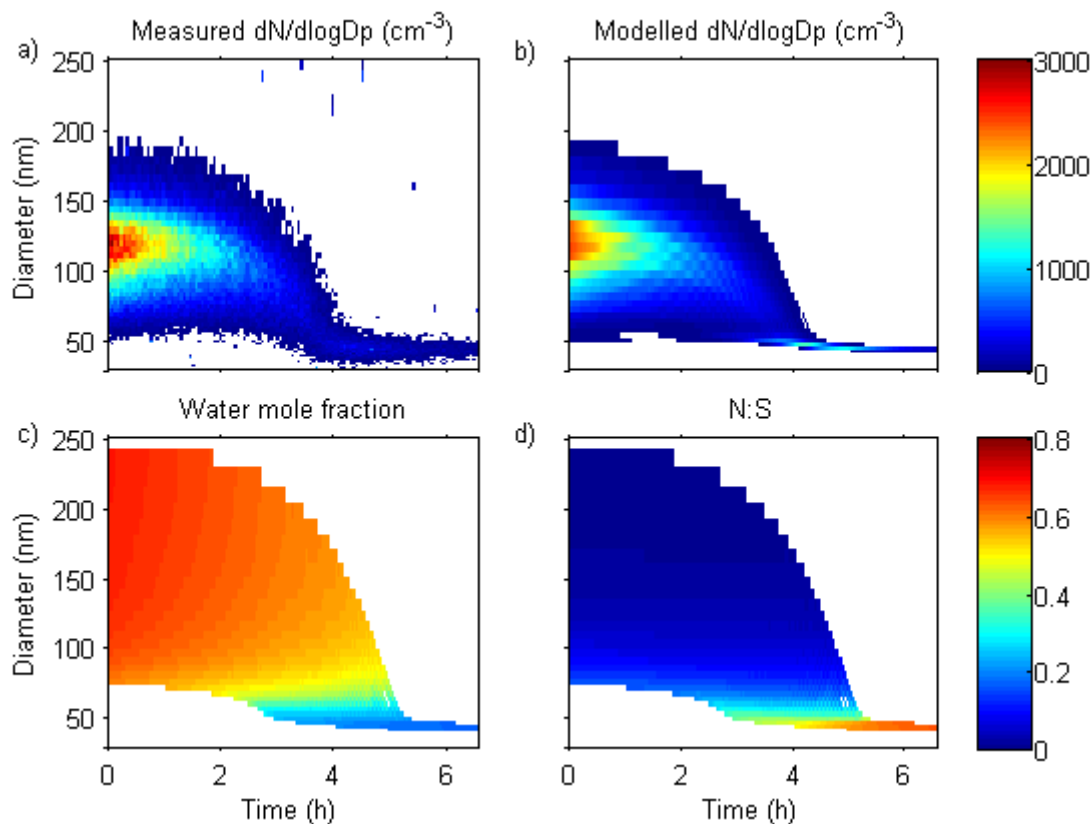
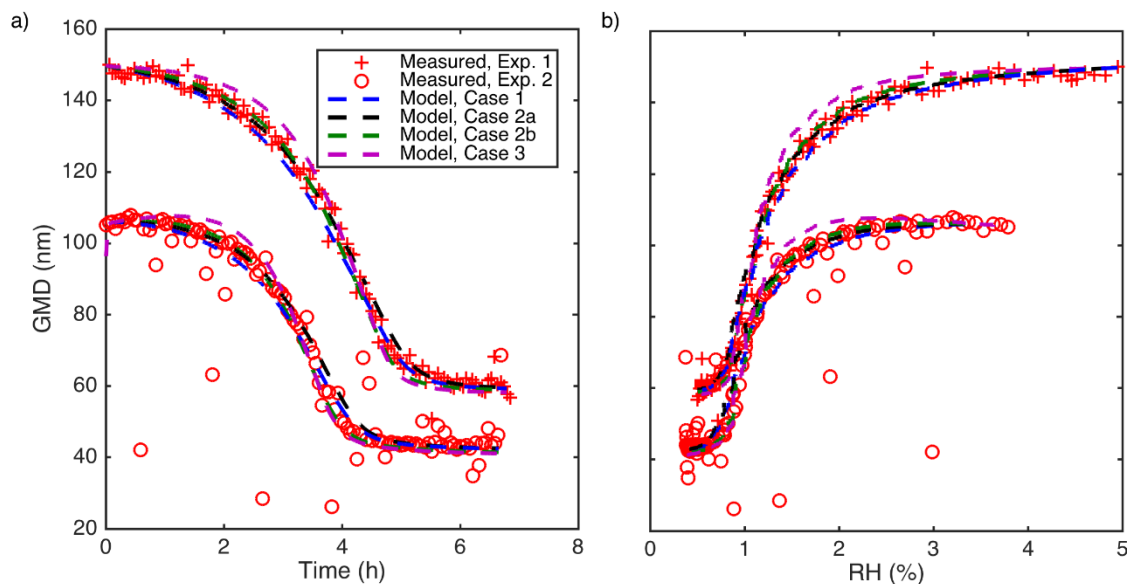


Figure 3. Particle shrinkage at low RH. Measured (a) and modelled (b) particle number size distribution evolution during experiment 2 performed at $T=288.8\text{ K}$ for Case 2a with $K_{H_2SO_4}=2.40\cdot 10^9\text{ mol}\cdot\text{kg}^{-1}$ and $^xK_{SO_3}=1.43\cdot 10^{10}$. Figures (c) and (d) show the modelled particle water mole fraction, χ_{H_2O} and N:S, respectively.



5 **Figure 4.** Modelled and measured GMD evolution as a function of (a) time and (b) RH for experiments 1 and 2 performed at $T=288.8$ K. The model results presented are from simulations 1–4 and 13–16 with NH_3 as a particle phase contaminant listed in Table 2 (Case 1 ($K_{\text{H}_2\text{SO}_4}=2.00 \cdot 10^9 \text{ mol} \cdot \text{kg}^{-1}$), Case 2a ($K_{\text{H}_2\text{SO}_4}=2.40 \cdot 10^9 \text{ mol} \cdot \text{kg}^{-1}$ and $^xK_{\text{SO}_3}=1.43 \cdot 10^{10}$), Case 2b ($K_{\text{H}_2\text{SO}_4}=4.00 \cdot 10^9 \text{ mol} \cdot \text{kg}^{-1}$ and $^xK_{\text{SO}_3}=1.54 \cdot 10^9$) and Case 3 ($K_{\text{H}_2\text{SO}_4}=1.00 \cdot 10^{11} \text{ mol} \cdot \text{kg}^{-1}$ and $^xK_{\text{SO}_3}=3.33 \cdot 10^7$)). The pure liquid saturation vapour pressures of H_2SO_4 and SO_3 are taken from Eq. 10, N–K–L parameterisation, (Kulmala and Laaksonen (1990) and Noppel et al., 2002) and Eq. 11 (Nickless, 1968), respectively.

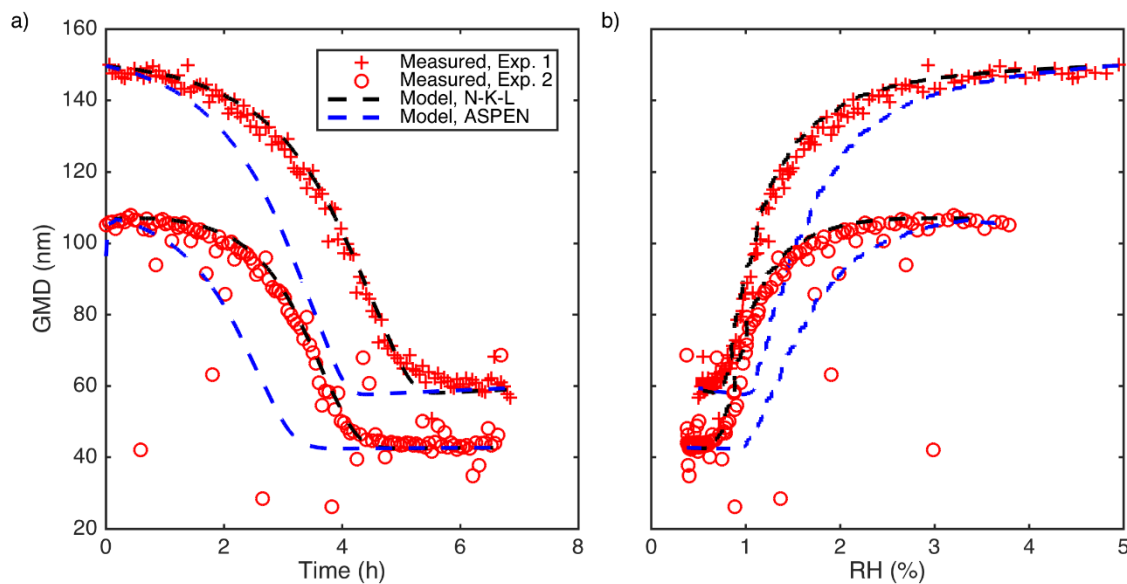
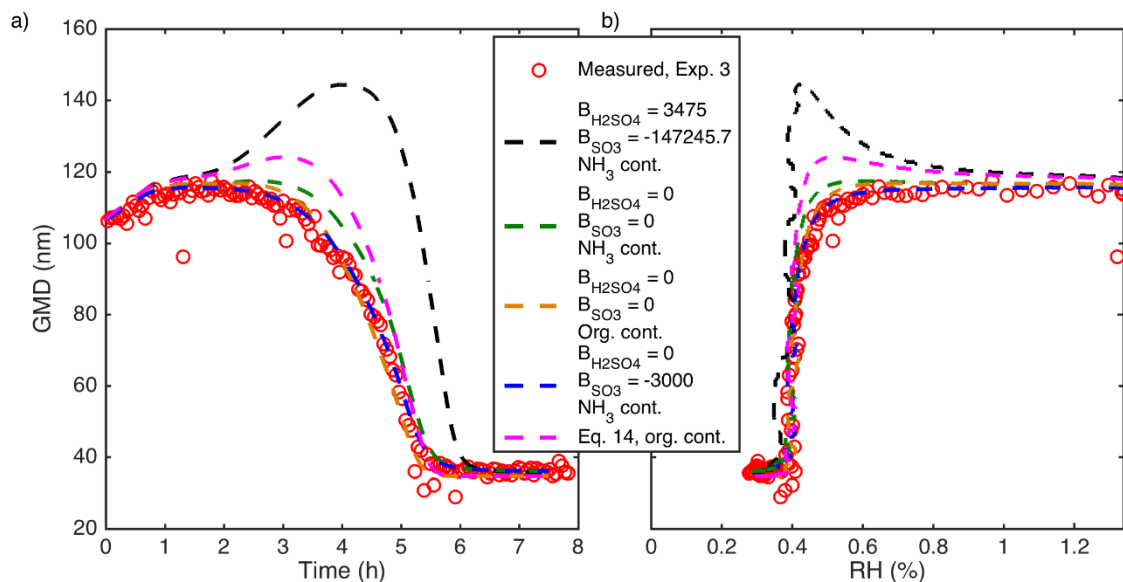


Figure 5. Modelled and measured GMD evolution as a function of (a) time and (b) RH for experiments 1 and 2 performed at $T=288.8$ K. The model results presented are from simulations 5, 12, 19 and 24 (for Case 1) listed in Table 2. The pure liquid saturation vapour pressure of H_2SO_4 is calculated with Eq. 10, N-K-L parameterisation, (Kulmala and Laaksonen, 1990 and Noppel et al., 2002) or with a parameterisation from the Aspen Plus Databank. The modelled particles are composed of S(VI), water and non-volatile and non-water-soluble organics. The H_2SO_4 activity is calculated with Eq. 14 using the tabulated chemical potentials from Giaque et al. (1960).

5

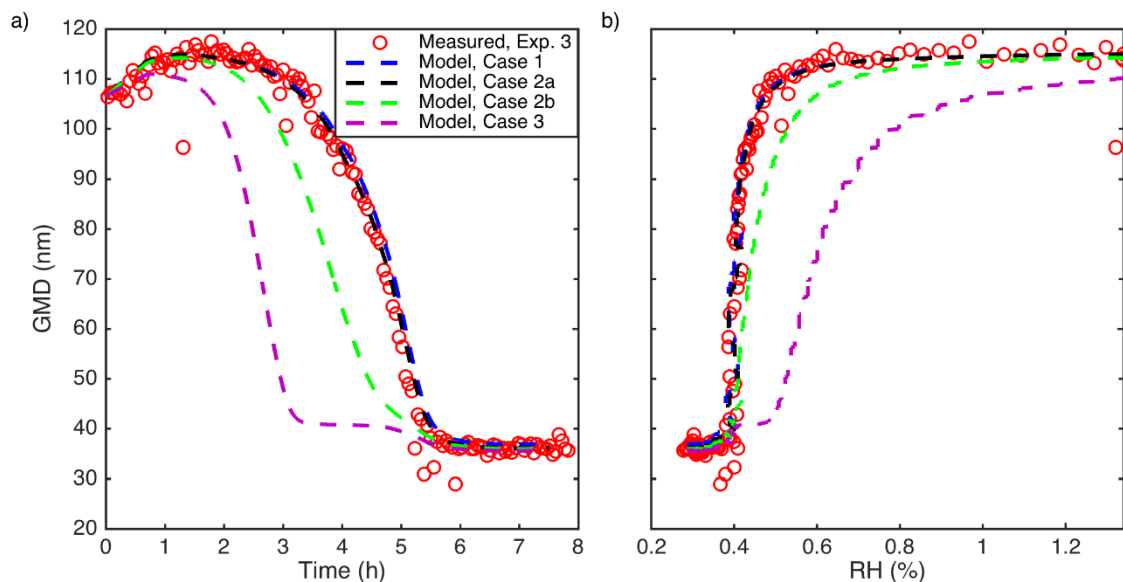
10



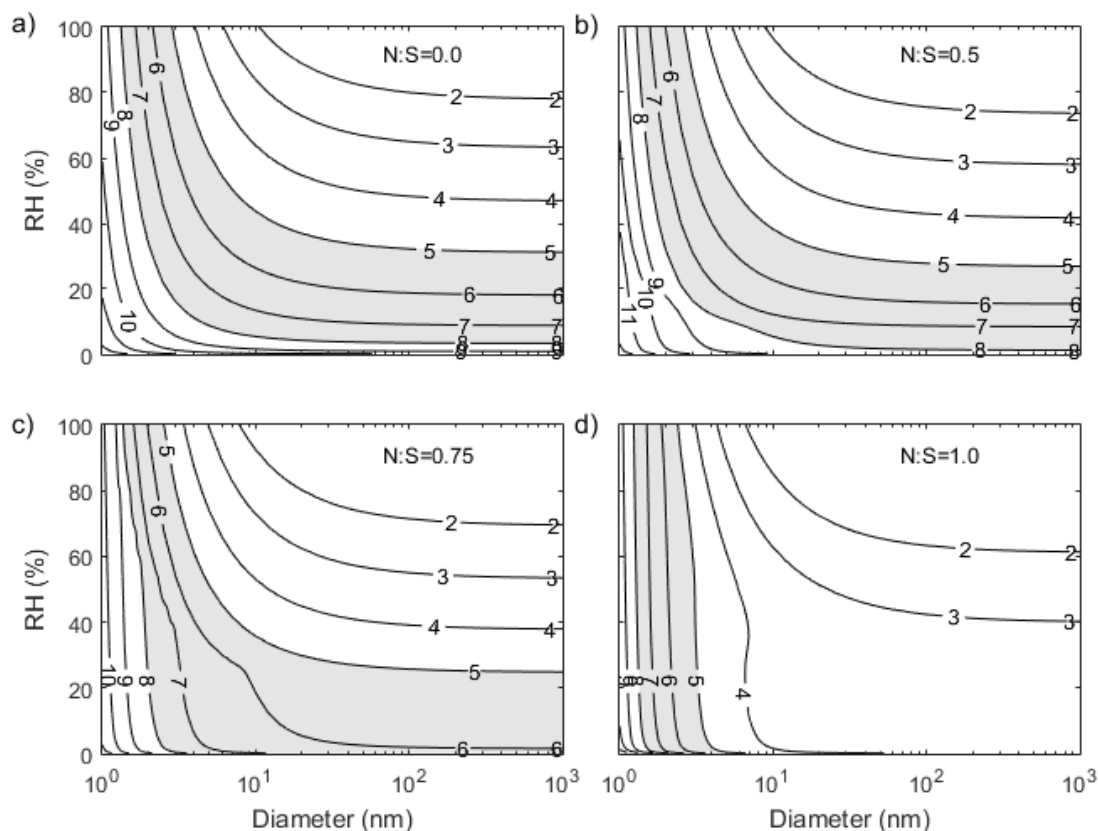
5 **Figure 6. Modelled and measured GMD evolution as a function of (a) time and (b) RH for experiment 3 performed at a temperature range from 268 K to 293 K. The pure liquid saturation vapour pressures of H₂SO₄ and SO₃ are calculated with Eq. 10 from Kulmala and Laaksonen (1990) and Noppel et al., 2002 and Eq. 11 from Nickless (1968), respectively. In all model simulations (29, 33, 34 and 36 listed in Table 2), except the one using Eq. 14, (simulation 28 listed in Table 2) $K_{H_2SO_4}=2.40 \cdot 10^9 \text{ mol} \cdot \text{kg}^{-1}$ and $^xK_{SO_3}=1.43 \cdot 10^{10}$ at $T=288.8 \text{ K}$ (Case 2a).**

10

15



5 **Figure 7. Modelled and measured GMD evolution as a function of (a) time and (b) RH for experiment 3 performed at temperature range from 268 K to 293 K. The model results presented are from simulations 50–53 listed in Table 2 (Case 1 ($K_{H_2SO_4}=3.80 \cdot 10^9 \text{ mol} \cdot \text{kg}^{-1}$), Case 2a ($K_{H_2SO_4}=4.00 \cdot 10^9 \text{ mol} \cdot \text{kg}^{-1}$ and $^xK_{SO_3}=4.55 \cdot 10^{10}$), Case 2b ($K_{H_2SO_4}=5.00 \cdot 10^9 \text{ mol} \cdot \text{kg}^{-1}$ and $^xK_{SO_3}=5.00 \cdot 10^9$) and Case 3 ($K_{H_2SO_4}=1.00 \cdot 10^{11} \text{ mol} \cdot \text{kg}^{-1}$ and $^xK_{SO_3}=5.00 \cdot 10^7$)). The pure liquid vapour pressures of H_2SO_4 and SO_3 were taken from Que et al., (2011) (original source Aspen Plus Databank).**



5 **Figure 8.** Modelled effective H_2SO_4 saturation concentration, $C^*_{\text{H}_2\text{SO}_4,\text{S}}$ (molecules $\cdot\text{cm}^{-3}$), expressed in $\log_{10}(C^*_{\text{H}_2\text{SO}_4,\text{S}})$, at $T=288.8\text{ K}$, $\text{RH } 0\text{--}100\%$ and particle diameters in the range from 1 to 10^3 nm . The contour $\log_{10}(C^*_{\text{H}_2\text{SO}_4,\text{S}})=7$ corresponds to $C^*_{\text{H}_2\text{SO}_4,\text{S}}=10^7\text{ molecules}\cdot\text{cm}^{-3}$. The grey shading indicates the atmospheric range of H_2SO_4 ($10^5\text{--}10^8\text{ cm}^{-3}$). Figure 8 provides the results for particles composed (a) only of S(VI) and H_2O ($N:S=0$), (b) with $N:S=0.5$, (c) with $N:S=0.75$ and (d) with $N:S=1$. The equilibrium constants are $K_{\text{H}_2\text{SO}_4}=2.40\cdot 10^9\text{ mol}\cdot\text{kg}^{-1}$ and ${}^xK_{\text{SO}_3}=1.43\cdot 10^{10}$. The pure liquid saturation vapour pressures of H_2SO_4 and SO_3 are calculated with Eq. 10 and 11.